Primjena homogenizacije prvog reda kod određivanja mehaničkog konstitutivnog modela ponašanja PBT smole

Jelušić, Toni

Master's thesis / Diplomski rad

2019

UNIVERSITY OF ZAGREB

FACULTY OF MECHANICAL ENGINEERING AND NAVAL ARCHITECTURE

MASTER'S THESIS

Toni Jelušić

Zagreb, 2019

UNIVERSITY OF ZAGREB

FACULTY OF MECHANICAL ENGINEERING AND NAVAL ARCHITECTURE

MASTER'S THESIS

APPLICATION OF THE FIRST-ORDER HOMOGENIZATION IN MODELLING OF CONSTITUTIVE MECHANICAL BEHAVIOUR OF PBT RESIN

Supervisor:	Student:
doc. dr. sc. Tomislav Lesičar	Toni Jelušić

Zagreb, 2019

I would like to state that I have written this thesis independently using the knowledge acquired during my undergraduate and graduate studies and the listed references.

I would like to express my thanks to my supervisor doc. dr. sc. Tomislav Lesičar for guidance during the writing of this thesis. With his help and suggestions, he greatly contributed to solving of all issues and problems that arose during the modeling phase.

Furthermore, I am thankful for all the advice received from prof. dr. sc. Zdenko Tonković. With his knowledge and experience, he contributed in formulating the concept of this thesis.

Special thanks to Mr. Ante Bubalo, mag. ing. mech., Product Engineer Simulation & Material & Patent Specialist at Yazaki Europe Limited - Zagreb Branch, for the provided experimental data.

Also, thanks to my family for the indirect support during my studies and the writing of this thesis.

Toni Jelušić

SVEUČILIŠTE U ZAGREBU
FAKULTET STROJARSTVA I BRODOGRADNJE
Središnje povjerenstvo za završne i diplomske ispite
Povjerenstvo za diplomske ispite studija strojarstva za smjerove:
procesno-energetski, konstrukcijski, brodostrojarski i inženjersko modeliranje i računalne simulacije

Sveučilište u Zagrebu Fakultet strojarstva i brodogradnje	
Datum 27-11-2019	Prilog
Klasa: 602-04/19-6/3	
Ur. broj: 15-1703-19-414	

DIPLOMSKI ZADATAK

Student: **Toni Jelušić** Mat. br.: 0035190821

Naslov rada na hrvatskom jeziku: **Primjena homogenizacije prvog reda kod određivanja mehaničkog konstitutivnog modela ponašanja PBT smole**

Naslov rada na engleskom jeziku: **Application of the First-Order Homogenization in Modelling of Constitutive Mechanical Behaviour of PBT Resin**

Opis zadatka:

Polybutylene terephthalate (PBT) is a material belonging into a group of crystal polymers (thermoplastics). It is produced by polymerisation of butadiene and terephthalic acid. By its mechanical properties, PBT is characteristic by high strength and ductility, as well as good stiffness in various atmospheric conditions. Furthermore, it is redundant to high temperatures and ageing. Also, it is known by low hygroscopy and very good electrical properties, as well as colour stability and chemicals resistance. Due to favourable mechanical characteristics, PBT is highly popular in the electrical and car industry. In the car industry, PBT is used for production of the car bumpers, door handles, wipers and various electrical connectors, which are the main product of the firm Yazaki Europe Limited. However, during the manufacturing process of PBT, porosities can appear inside of the material, having high impact on mechanical behaviour of the PBT.

This master thesis will focus on the determination of the influence of the porosities on the mechanical response of the PBT. Based on the facts stated in the text above, in this study it is necessary to:

1. Study available literature on the homogenization methods for modelling of mechanical behaviour of heterogeneous materials.
2. Determine the necessary Representative Volume Element (RVE) size and geometry of a PBT consisting of various porosity ratio. Apply periodic boundary conditions.
3. Obtain linear elastic response, yield stress and elastoplastic regime of a PBT consisting of various porosity ratio using homogenization methodology.
4. If possible, validate the numerical results by comparison to the experimental measurements.

During thesis preparation one must comply with the standard rules for preparation of master thesis. It is necessary to list all literature used and received assistance.

Zadatak zadan:	Datum predaje rada:	Predviđeni datum obrane:
26. rujna 2019.	28. studenoga 2019.	2. – 6. prosinca 2019.

Zadatak zadao:

Doc. dr. sc. Tomislav Lesičar

Predsjednica Povjerenstva:

Tanja Jurčević Lulić

Prof. dr. sc. Tanja Jurčević Lulić

Contents

List of Figures

List of Tables

Symbols and Abbreviations

Latin symbols

Symbol	**Unit**	**Description**
$\mathbf{a}$	[-]	vector of polynomial coefficients
A	[mm^2]	section area
$\mathbf{A}^{\varepsilon}$	[-]	strain concentration tensor
$\mathbf{B}^{\varepsilon}$	[-]	strain concentration tensor
C	[MPa]	stiffness
$\mathbf{C}$	[MPa]	elasticity matrix
$\overline{\mathbf{C}}$	[MPa]	macro stiffness
$\mathbf{C}^{\mathrm{alg}}$	[-]	algorithmic tangent operator
$\mathbf{C}^{\mathrm{ep}}$	[-]	continuum tangent operator
d	[mm]	diameter
E	[MPa]	Young's modulus
$\mathbf{E}$	[mm/mm]	uniform remote strain
F	[MPa]	proportionality constant
G	[MPa]	shear modulus
$\mathbf{H}^{\varepsilon}\left(I, \mathbf{C}_0, \mathbf{C}_1\right)$	[-]	single inclusion strain concentration tensor
$\mathbf{I}$	[-]	fourth-rank identity tensor
J_2	[-]	J_2 plasticity
K	[-]	strain hardening modulus
k	[-]	isotropic hardening coefficient
l	[mm]	length
m	[-]	isotropic hardening exponent

n	[-]	strain hardening exponent
$\mathbf{N}$	[-]	vector of shape functions
p	[mm/mm]	plastic strain
$R(p)$	[MPa]	hardening stress
S	[MPa]	engineering stress
$\boldsymbol{S}$	[mm^2/N]	compliance matrix
t	[mm]	thickness
u	[mm]	displacement
$\boldsymbol{u}$	[mm]	displacement vector on the RVE boundary
$\mathbf{u}$	[mm]	displacement vector
V	[m^3]	volume
$\mathbf{v}$	[mm]	vector of nodal displacements
w	[mm]	width

Greek symbols

Symbol	**Unit**	**Description**
α	[-]	hardening parameter
$\boldsymbol{\alpha}$	[-]	matrix of polynomials
ε	[-]	tolerance
ε^*	[mm/mm]	stress-free eigenstrain
ε^∞	[mm/mm]	far field strain
$\boldsymbol{\varepsilon}$	[mm/mm]	strain
$\langle\boldsymbol{\varepsilon}\rangle_\omega$	[MPa]	volume average of strain
ε^{e}	[mm/mm]	elastic strain

ε^{p}	[mm/mm]	plastic strain
$\varepsilon^{\mathrm{tot}}$	[mm/mm]	total strain
ε_{ϵ}	[mm/mm]	engineering strain
$\boldsymbol{\varepsilon}(\mathbf{X})$	[mm/mm]	macro strain
ν	[-]	Poisson's ratio
ν_i	[-]	volume fraction of phase i
σ	[MPa]	stress
σ_{I}, σ_{II}, σ_{III}	[MPa]	principal stress
$\langle\boldsymbol{\sigma}\rangle_{\omega}$	[MPa]	volume average of stress
$\boldsymbol{\sigma}(\mathbf{X})$	[MPa]	macro stress
σ_{eq}	[MPa]	equivalent stress
$\sigma_{\mathrm{eq}}^{\mathrm{tr}}$	[MPa]	elastic predictor
σ_Y	[MPa]	yield strength
$\zeta\left(I, \mathbf{C}_0\right)$	[-]	Eshelby's tensor

Abbreviations

Abbreviation	**Meaning**
1D	one-dimensional
2D	two-dimensional
3D	three-dimensional
BC	boundary condition
EIP	equivalent inclusion problem
FE	finite element
FEA	finite element analysis
FEM	finite element method
GF	glass fiber
MF	mean-field
MFH	mean-field homogenization
MT	Mori-Tanaka
ODF	orientation distribution function
PBT	Polybutylene Terephthalate
PMC	polymer matrix composite
RVE	representative volume element

Summary

The goal of this thesis is to determine the effect of pores on the stiffness of the material used for manufacturing of automotive connectors. A representative material model was generated to account for the nonlinear properties which are a result of the presence of pores in the material used: Polybutylene Terephthalate (PBT).

The model was established through the use of a representative volume element (RVE) and periodic boundary conditions. The RVE is a statistically representative sample of the microstructure of the material. The RVE is seen as a composite material, which is composed of an elasto-plastic matrix (PBT) and a certain volume fraction of inclusions (pores). It was shown that the pore fraction affects the strength of the material; with more pores present, the strength of material, together with maximum strain values, was lower for the same loads and boundary conditions. By knowing the fact that the material under investigation has excellent thermal properties, which is one of the reasons why it is used in underhood applications, a thermal analysis was omitted because there is no indication that temperature affects its mechanical properties significantly.

For the modeling of the material, the first-order homogenization approach was used, primarily the Mori-Tanaka method. This approach made it possible to obtain macro stresses and strains, which gave an indication of the actual behavior for the material at hand. With this approach, the material response could be predicted with enough accuracy, while lowering the computational cost compared to a direct FE analysis. The obtained results were compared to experimental data.

Key words: Polybutylene Terephthalate (PBT), homogenization, multi-scale approach, RVE, porosity, anisotropy, micro-level, macro-level, composite materials

Prošireni sažetak (Abstract in Croatian)

U ovom radu pokazana je primjena homogenizacije u modeliranju konstitutivnog mehaničkog modela PBT smole. Homogenizacija se primjenjuje za modeliranje heterogenih materijala koji pokazuju nelinearno ponašanje. U tu skupinu spadaju materijali u kojima je prisutna poroznost i kompozitni materijali. Pri modeliranju ponašanja tih materijala, promatra se njihova mikrostruktura. Zbog eksplicitnog modeliranja mikrostrukture na mikrorazini javlja se anizotropija, koja nakon homogenizacije na markorazini daje izotropno ponašanje. Ovdje se homogenizacija primarno koristi kako bi se uzeo u obzir utjecaj poroznosti na mehanička svojstva PBT smole.

Nakon uvodnog prvog poglavlja u kojem je dan pregled rada, po poglavljima su redom opisani: svojstva PBT smole, materijalni model korišten pri modeliranju PBT smole, homogenizacija i njena primjena, osnove metode konačnih elementa te rezultati analize mehaničkog ponašanja PBT smole.

U drugom poglavlju je ukratko opisan polibutilen tereftalat (PBT). Zbog svojih iznimnih mehaničkih, termalnih, kemijskih i električnih svojstava, PBT se koristi u raznim granama industrije, a osobito u automobilskoj industriji. PBT se često ojačava staklenim vlaknima i dvije najčešće varijante su PBT ojačan s 20% vlakana (PBT-GF20) i PBT ojačan s 30% vlakana (PBT-GF30).

U trećem poglavlju je opisan materijalni model koji je korišten pri modeliranju ponašanja PBT-a. U uvodu je dan pregled osnovnih konstitutivnih jednadžbi s naglaskom na anizotropnost materijala. Potom je opisan elasto-plastični materijalni model koji se temelji na von Mises-ovom kriteriju tečenja.

U četvrtom poglavlju su izložene osnove homogenizacije. Uveden je pojam reprezentativnog volumnog elementa (RVE). RVE predstavlja uzorak mikrostrukture materijala čijom se analizom može utvrditi ponašanje cijelog modela. Da bi to bilo moguće, definirani su periodični rubni uvjeti. Periodični rubni uvjeti nameću deformaciju s makro razine na rubove RVE-a pri čemu se nameće kinematičko ograničenje na polje pomaka između dviju suprotnih strana RVE-a. Na kraju je opisana Mori-Tanaka metoda koja se vrlo često koristi za homogenizaciju dvofaznih materijala.

U petom poglavlju je ukratko opisana metoda konačnih elemenata. Dan je prikaz korištenih elemenata pri diskretizaciji simulacijskih modela. Za svaki korišteni element

opisana su njegova osnovna svojstva.

U šestom poglavlju je prikazana analiza mehaničkog ponašanja PBT-a te je promatran utjecaj poroznosti na spomenuta svojstva. Određeni su parametri potrebni za definiranje materijalnog modela. Prvo je izvršena verifikacija rezultata dobivenih simulacijom RVE-a. Potom je napravljena usporedba s rezultatima koji su dobiveni pomoću Mori-Tanaka metode i rezultatima dobivenim direktnom simulacijom epruvete gdje se u svakom iteracijskom koraku vrši homogenizacija materijalnih svojstava. Na kraju je za PBT B1305 napravljena usporedba rezultata višerazinske simulacije s eksperimentalnim rezultatima.

Konačno, u sedmom poglavlju dan je osvrt na prikazanu analizu i rezultate. Objašnjen je utjecaj različitih parametara na dobivene rezultate i dani su prijedlozi za daljnje istraživanje.

1 Introduction

Automotive connectors are components which provide an interface between two subsystems. Usually, they are used to connect electric wiring and other electric components like circuit boards and batteries. With higher demands in terms of cost, size, weight and performance, improved materials are used in the manufacturing process of such connectors. With that, new challenges arise in the optimization of connectors made from those materials. For such applications, polymers and fiber-reinforced composite materials, usually polymer matrix composites (PMC), are mostly used. Composites are particularly interesting, especially in the automotive industry, because of their superior mechanical properties, the ability to create various materials with desired properties for a specific application and weight savings in the range of 30-70% for some suspension and power train components [1]. The behavior of polymer materials will be the matter of investigation of this thesis.

The material used for manufacturing of the connector component is usually one of the following variants of Polybutylene Terephthalate (PBT): non-reinforced PBT resin, and PBT reinforced with glass fibers. Out of the two, the non-reinforced PBT resin was tested to obtain the response under the usual loading conditions. The properties of the material are described in more detail in Chapter 2.

The motivation for this investigation was to study the effect of pores on the strength of the material. When pores are present, a numerical analysis for the assumption of a homogeneous and isotropic material does not yield valid results. The occurrence of pores is tied with the injection molding process used during manufacturing. During the injection molding process, air bubbles may ensue which leads to an overall lower strength and degradation of the material. If fibers are added, some might be misaligned and some may even break. This is disadvantageous because there is no accurate way to determine the orientation of the fibers once the molding process has finished. Therefore, a case study is carried out to determine the actual maximum loads the component with lowered mechanical properties can handle before failure occurs.

For this purpose, the assumption that the material is heterogeneous and anisotropic is made, with the goal being to predict the actual behavior of the component that is comparable with experimental results. The term anisotropy refers to a characteristic of real materials where it is assumed that the material properties are not equal in all directions and in all sections of the material, i.e. the material is not locally homogeneous. An elasto-plastic material model is used for the component and more details about it can be found in Chapter 3.

With heterogeneity in mind, a micro-mechanical approach was employed together with homogenization methods for the purpose of obtaining the actual response of the material. Homogenization methods were used because of their simplicity, lower computational costs, and the fact that one requires only the material properties of composite's constituents, thus eliminating the requirement to obtain the properties of the composite [2]. For this purpose, the Digimat software suite was used, which makes it possible to predict nonlinear behavior of anisotropic and composite materials. In this thesis, first-order homogenization methods were primarily used and more details about these methods can be found in Chapter 4.

With the concept of a representative volume element (RVE), homogenization methods are coupled with the finite element analysis. This approach consists of generation of a representative volume element of the material microstructure, which is then used as a model in a finite element analysis. The obtained results of stress distribution on the RVE are then homogenized to obtain the volume average values, thus giving the homogenized response of the material. The fundamentals of finite element method and the finite element model are laid out in Chapter 5.

Finally, Chapter 6 shows the obtained results. Various parameters were tested to see their effect on the behavior of the material. Size variation of the RVE was carried out to generate RVEs which include different number of pores to observe at which number of pores the microstructure becomes statistically representative. Different random geometries were generated to show that random geometry has no effect on the obtained response. The results obtained by small strain theory were compared to the results obtained by employment of the large strain approach. In the end, the predicted mechanical response obtained through a representative volume element was compared to experimentally obtained stress-strain curves of PBT 1305.

2 Material

2.1 Introduction

An overview of PBT and its properties is given. Furthermore, injection molded PBT reinforced with 20 and 30 percent of glass fibers is described.

2.2 Polybutylene Terephthalate (PBT)

"Polybutylene Terephthalate (PBT) is a semi-crystalline engineering thermoplastic material. ... PBT is produced by polycondensation of terephthalic acid or dimethyl terephthalate with 1,4-butanediol using special catalysts", [3]. The chemical formula of Polybutylene Terephthalate is $(C_{12}H_{12}O_4)n$ and the molecular structure of PBT is shown in Figure 2.1.

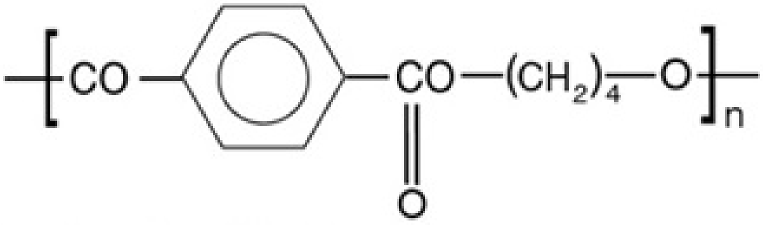

Figure 2.1: Molecular structure of Polybutylene Terephthalate [3]

Because of its outstanding properties, PBT has a wide range of use in automotive industry, electrical and electronic industry and in medicine. The PBT polymer is predominantly used as a material for electrical components in automotive industry, especially underhood applications, because of its excellent mechanical, thermal, chemical and electrical properties [3]. The components that are usually made of PBT include: connectors, fans, mirror housings, fuel system components, sensor housings and fuse boxes. PBT components are usually manufactured by a process called injection molding.

With regard to its mechanical properties, it stands out with its excellent machining characteristics, reduced weight and cost of components, high strength, good creep resistance, toughness and stiffness [3]. The main advantages of PBT are its ability to withstand thermal stress and high chemical resistance which is the reason it is used as a material for the connector component. Therefore, it is expected that temperature will not play a significant role in the loading of the component and the thermal analysis will be omitted from this thesis.

Polybutylene Terephthalate also has outstanding electrical properties, serving as a protector of electrical and electronic components and can block UV radiation. Although PBT exhibits great mechanical, thermal and electric properties, it does not come without limitations. Some of them are high mold shrinkage, sensitivity to hot water and notch sensitive unreinforced PBT. A more detailed overview of Polybutylene Terephthalate can be found in [3].

2.2.1 Mechanical properties of PBT

For this certain application, we are mostly interested in the mechanical properties of PBT. The material used is produced by one of the leading specialty chemicals suppliers worldwide, Lanxess, with its brand Pocan. The mechanical properties of Pocan B1305 000000 are shown in Table 2.1.

Table 2.1: Mechanical properties of PBT, non-reinforced, injection molding [4]

Tensile modulus	2800 MPa
Stress at break	60 MPa
Strain at break	9 %
Tensile creep modulus, 1h	2400 MPa
Tensile creep modulus, 1000h	1400 MPa
Density	1310 kg/m^3

Temperature dependent stress-strain curves for PBT obtained experimentally can be seen in Figure 2.2.

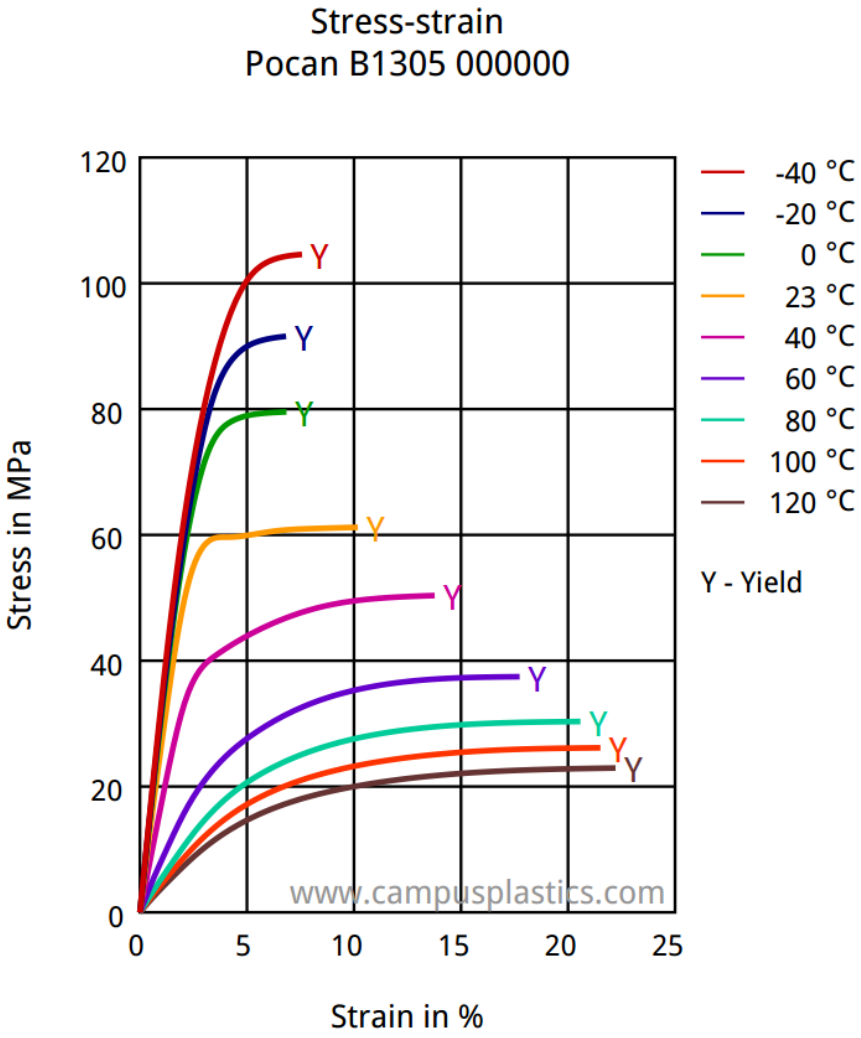

Figure 2.2: Stress-strain curves of PBT for various temperatures [4]

2.3 Glass reinforced PBT

Because the tensile strength and the yield strength are too low if pure PBT is used, the material is reinforced with glass fibers. This way a material which is a lot more capable of handling higher stresses is obtained. Compared to the Young's modulus of PBT which is somewhere between 2-3 GPa, with the reinforcement of 20 percent glass fibers the value becomes 7.1 GPa which shows a two- to threefold increase in strength.

In the linear elastic case, the radius of inclusions does not affect the strength of the material. The shape of inclusions has to be defined properly, because it has a major effect on mechanical properties. On the other hand, if an elasto-plastic material model is used, it is expected that the size of inclusions will have a significant effect. The longer the fibers are, the higher the tensile strength will be. The mechanical properties of Polybutylene Terephthalate (PBT), reinforced with glass fibers with a volume fraction of 20 percent and produced with injection molding, labeled as Pocan B3225 000000, are shown in Table 2.2.

Table 2.2: Mechanical properties of PBT, 20 % glass fibers, injection molding [5]

Tensile modulus	7100 MPa
Stress at break	120 MPa
Strain at break	3.4 %
Tensile creep modulus, 1h	6900 MPa
Tensile creep modulus, 1000h	6300 MPa
Density	1460 kg/m^3

Temperature-dependent stress-strain curves of PBT-GF20 are shown in Figure 2.3.

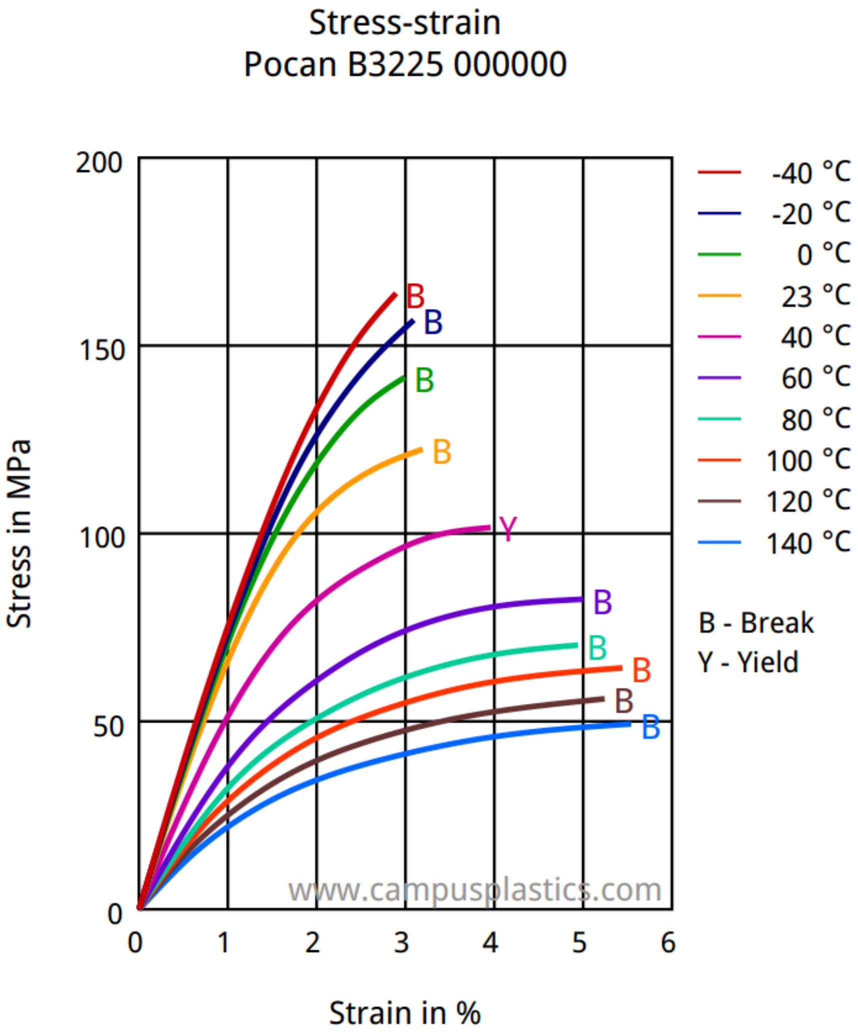

Figure 2.3: Stress-strain curves of PBT-GF20 for various temperatures [5]

To define the microstructure of PBT-GF20, mechanical properties of the matrix and the mechanical properties together with shape of inclusions are needed. The tensile modulus of the PBT matrix is $E = 2800$ MPa [4], and the Poisson's ratio of PBT is $\nu = 0.3902 - 0.406$ [6]. The inclusions are glass fibers E-Glass with a tensile modulus of $E = 72400$ MPa and a Poisson's ratio of $\nu = 0.21 - 0.23$. The size and shape of the fiber are determined with the length and diameter of the fiber. It is assumed that the fibers are sphero-cylindrical. The fiber diameter is $d = 14$ μm and the fiber length is $l = 150$ μm [7, 8]. All properties are shown in Table 2.3.

Table 2.3: Mechanical properties of PBT & E-Glass

Material	E [MPa]	ν [-]
PBT	2800	0.3902-0.406
E-Glass	72400	0.21-0.23

It is important to note that the fiber length is an average estimate of all fibers, because in reality, not all fibers will be of equal length. It is also possible that some of the fibers break in the process of injection molding into the polymer matrix (PBT). This has to be taken into account during the prediction of the real behavior of the new-formed material, because it is expected that this will have an effect on the solution obtained with numerical analysis; i.e. there will be a discrepancy in experimental and numerical results.

The material properties of glass reinforced PBT, with a volume fraction of glass fibers of 30 percent, denoted as Pocan B3235 000000, can be found in [9].

Table 2.4: Mechanical properties of PBT, 30 % glass fibers, injection molding [9]

Tensile modulus	9800 MPa
Stress at break	140 MPa
Strain at break	2.9 %
Tensile creep modulus, 1h	9800 MPa
Tensile creep modulus, 1000h	8900 MPa
Density	1550 kg/m^3

Figure 2.4 shows the experimentally obtained stress-strain curves for PBT-GF30.

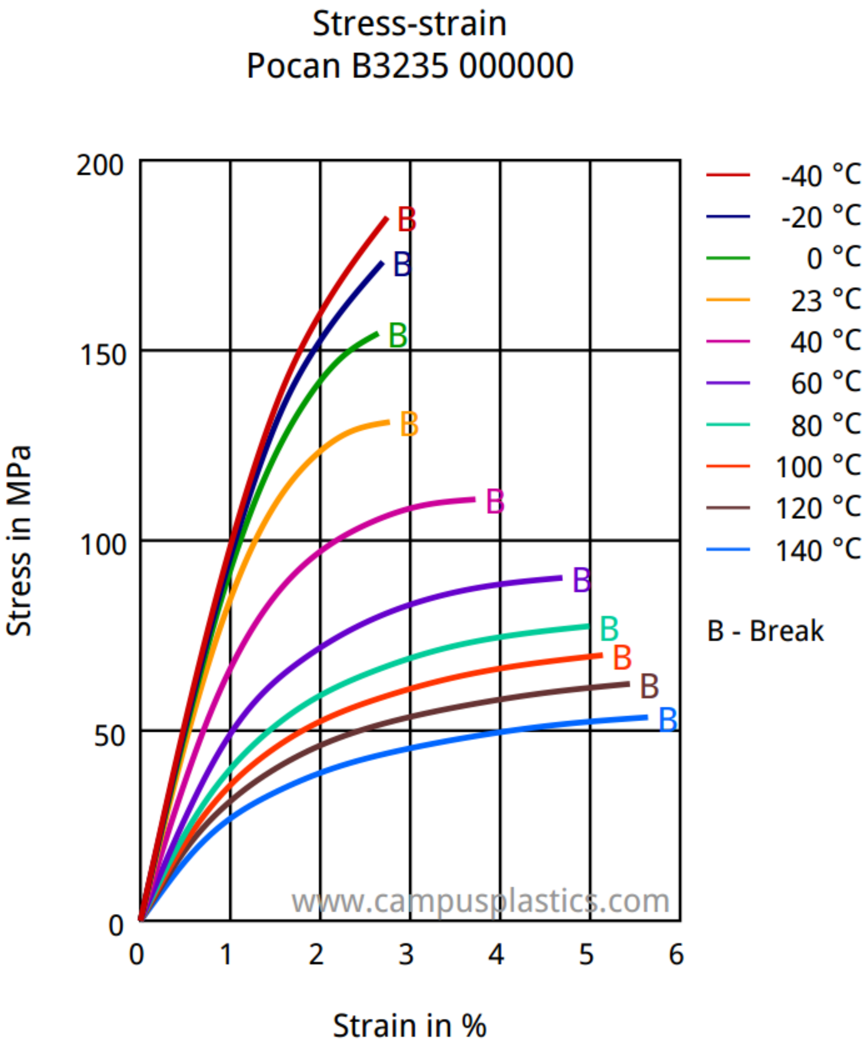

Figure 2.4: Stress-strain curves of PBT-GF30 for various temperatures [9]

PBT, especially the variant reinforced with 30% of fibers, is hard and rigid, and its ability of withstanding dynamic load at wide range of temperature makes it a material of choice for designing mounting brackets and control module casings for automotive lamps. For lamps installed near vehicle exhaust or in areas with extreme temperatures, PBT-GF30 is the most suitable material [10]. Finally, for reference, Figure 2.5 shows a representative microstructure of PBT reinforced with 30 percent of glass fibers.

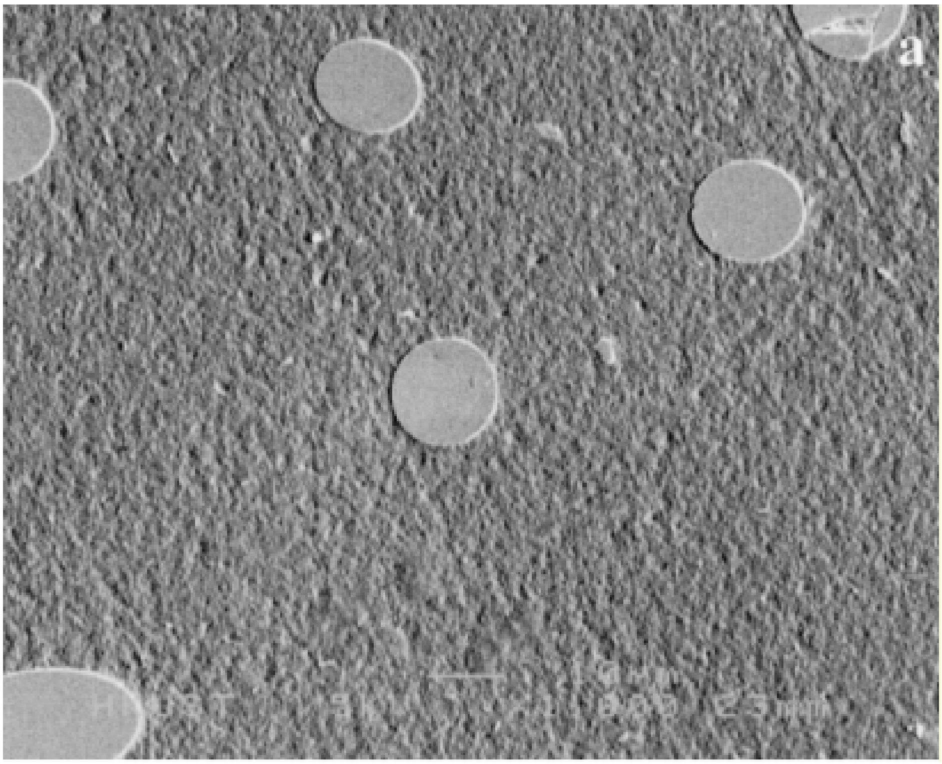

Figure 2.5: Microstructure of PBT reinforced with 30% of glass fibers [11]

2.4 Summary

An overview of Polybutylene Terephthalate is given. This material has a wide range of use in the automotive industry because of its outstanding properties. It can be reinforced with glass fibers (usually 20 and 30 percent) to form a composite material which has more desirable properties for a particular application. Out of the three variations (non-reinforced PBT, PBT reinforced with 20 or 30 percent glass fibers), the first one will be the primary focus of this investigation. Analysis of PBT's microstructure and the effect of pores on its properties will be conducted and shown in Chapter 6.

3 Material model

3.1 Introduction

To define a material model means to find the constitutive matrix that correlates stresses and strains. This is a simple task for elastic materials, but if a heterogeneous anisotropic material is studied, complications may arise. Therefore, the nonlinear response of heterogeneous materials is determined by means of homogenization methods. This is achieved through the constitutive matrix of homogenized material which describes the relation between macro stresses and strains. In the following section the basic relations of elasticity theory are shown.

3.2 Anisotropy

When the material with its microstructural properties has to be modeled, it can no longer be assumed that the material is ideal, homogeneous and isotropic. In this case, it is assumed that the material is anisotropic. Anisotropy describes the material whose properties are not evenly distributed in all directions.

Generally, the stress-strain relation for linear elastic anisotropic materials is presented in matrix form as in equation (3.1). This form is obtained by using the contracted notation where indices are mapped to obtain a simpler form. This equation is known as the generalized Hooke's Law.

$$\begin{bmatrix} \sigma_1 \\ \sigma_2 \\ \sigma_3 \\ \sigma_4 \\ \sigma_5 \\ \sigma_6 \end{bmatrix} = \underbrace{\begin{bmatrix} C_{11} & C_{12} & C_{13} & C_{14} & C_{15} & C_{16} \\ C_{21} & C_{22} & C_{23} & C_{24} & C_{25} & C_{26} \\ C_{31} & C_{32} & C_{33} & C_{34} & C_{35} & C_{36} \\ C_{41} & C_{42} & C_{43} & C_{44} & C_{45} & C_{46} \\ C_{51} & C_{52} & C_{53} & C_{54} & C_{55} & C_{56} \\ C_{61} & C_{62} & C_{63} & C_{64} & C_{65} & C_{66} \end{bmatrix}}_{\boldsymbol{C}} \begin{bmatrix} \varepsilon_1 \\ \varepsilon_2 \\ \varepsilon_3 \\ \varepsilon_4 \\ \varepsilon_5 \\ \varepsilon_6 \end{bmatrix} \tag{3.1}$$

The matrix $\boldsymbol{C}$ is obtained through the reduction of the number of components of the fourth-order stiffness tensor C_{ijkl} from equation (3.2). The tensor C_{ijkl} has 81 components, but those can be reduced to only 36 independent components. This is possible because the stress and strain tensors are symmetric ($\sigma_{ij} = \sigma_{ji}$, $\varepsilon_{kl} = \varepsilon_{lk}$). If (3.2) is rewritten as (3.3), (3.4) has to hold true, thus showing that the tensor C_{ijkl} is symmetric.

$$\sigma_{ij} = C_{ijkl}\varepsilon_{kl} \tag{3.2}$$

$$\sigma_{ji} = C_{jilk}\varepsilon_{lk} \tag{3.3}$$

$$C_{ijkl} = C_{jikl} = C_{ijlk} = C_{jilk} \tag{3.4}$$

In equation (3.1), the material constant C_{ij} is called stiffness, and the matrix $\boldsymbol{C}$ is called the elasticity matrix. The elasticity matrix relates the stresses and strains. Through the derivation of the strain energy function, it can be shown that the elasticity matrix has to be symmetric. This means that 15 non-diagonal constants are independent, resulting in the reduction of the number of independent elastic constants from 36 to 21 in the most general case of anisotropic elasticity [12, 13].

To obtain the compliance matrix $\boldsymbol{S}$ the inverse form of the elasticity matrix has to be found. The compliance matrix expresses the explicit relation of strains as a function of stresses. This matrix is also symmetric and it can be written as shown in (3.5).

$$\begin{bmatrix} \varepsilon_1 \\ \varepsilon_2 \\ \varepsilon_3 \\ \varepsilon_4 \\ \varepsilon_5 \\ \varepsilon_6 \end{bmatrix} = \underbrace{\begin{bmatrix} S_{11} & S_{12} & S_{13} & S_{14} & S_{15} & S_{16} \\ & S_{22} & S_{23} & S_{24} & S_{25} & S_{26} \\ & & S_{33} & S_{34} & S_{35} & S_{36} \\ & & & S_{44} & S_{45} & S_{46} \\ & & & & S_{55} & S_{56} \\ & & & & & S_{66} \end{bmatrix}}_{\boldsymbol{S}} \begin{bmatrix} \sigma_1 \\ \sigma_2 \\ \sigma_3 \\ \sigma_4 \\ \sigma_5 \\ \sigma_6 \end{bmatrix} \tag{3.5}$$

Frequently, an idealized material is used where it is assumed that the properties of the material are independent regarding to orientation. Such materials have an infinite number of symmetry planes. Materials that have such properties are called isotropic materials. An elastic material is considered isotropic when the loading direction has no effect on its material properties. Linear elastic isotropic materials have the elasticity matrix as shown in equation (3.6).

$$\begin{bmatrix}\sigma_1\\ \sigma_2\\ \sigma_3\\ \sigma_4\\ \sigma_5\\ \sigma_6\end{bmatrix} = \begin{bmatrix} C_{11} & C_{12} & C_{12} & 0 & 0 & 0\\ & C_{11} & C_{12} & 0 & 0 & 0\\ & & C_{11} & 0 & 0 & 0\\ & & & \dfrac{C_{11}-C_{12}}{2} & 0 & 0\\ & & & & \dfrac{C_{11}-C_{12}}{2} & 0\\ & & & & & \dfrac{C_{11}-C_{12}}{2}\end{bmatrix} \begin{bmatrix}\varepsilon_1\\ \varepsilon_2\\ \varepsilon_3\\ \varepsilon_4\\ \varepsilon_5\\ \varepsilon_6\end{bmatrix} \tag{3.6}$$

It can be seen that there are only two independent material constants in the elasticity matrix of isotropic materials. If the inverse of the elasticity matrix for isotropic materials is found, the compliance matrix can be written in terms of Poisson's ratio (ν) and Young's modulus (E). If the assumption of isotropy holds, by using those two parameters the shear modulus G can be expressed as:

$$G = \frac{E}{2(1+\nu)}. \tag{3.7}$$

Then the following compliance matrix is obtained:

$$\boldsymbol{S} = \frac{1}{E}\begin{bmatrix} 1 & -\nu & -\nu & 0 & 0 & 0\\ & 1 & -\nu & 0 & 0 & 0\\ & & 1 & 0 & 0 & 0\\ & & & 2(1+\nu) & 0 & 0\\ & & & & 2(1+\nu) & 0\\ & & & & & 2(1+\nu)\end{bmatrix}. \tag{3.8}$$

From that, the inverse matrix which is the elasticity matrix (3.10), where the constants C_{11} and C_{12} can also be expressed in terms of the Poisson's ratio and Young's modulus, can be determined.

$$C_{11} = \frac{E(1-\nu)}{(1+\nu)(1-2\nu)}, \quad C_{12} = \frac{E\nu}{(1+\nu)(1-2\nu)}. \tag{3.9}$$

$$\boldsymbol{C} = \frac{E}{(1+\nu)(1-2\nu)} \begin{bmatrix} 1-\nu & \nu & \nu & 0 & 0 & 0 \\ \nu & 1-\nu & \nu & 0 & 0 & 0 \\ \nu & \nu & 1-\nu & 0 & 0 & 0 \\ 0 & 0 & 0 & \dfrac{1-2\nu}{2} & 0 & 0 \\ 0 & 0 & 0 & 0 & \dfrac{1-2\nu}{2} & 0 \\ 0 & 0 & 0 & 0 & 0 & \dfrac{1-2\nu}{2} \end{bmatrix} \tag{3.10}$$

This matrix is generated when an anisotropic material is defined and modeled with the use of Digimat MF and FE modules. Those modules simplify the modeling process of anisotropic materials in a way that the mean-field linear elastic isotropic representation of the anisotropic material is generated. For example, if a material consists of n multiple phases, each with it's own stiffness C_1, C_2, ..., C_n, an isotropic representation of the nonlinear material can be generated with the use of homogenization methods. This way an elasticity matrix C_0 can be obtained, which defines a representative linear elastic isotropic material, in the form of the matrix from equation (3.6). A detailed overview can be found in [12].

3.3 Plasticity model

J2-plasticity model is used as the constitutive model. The foundation for this model is the equivalent von Mises stress σ_{eq} which is given by the equation (3.11).

$$\sigma_{\text{eq}} = \sqrt{J_2(\sigma)} = \left(\frac{3}{2}\mathrm{s} : \mathrm{s}\right)^{1/2}, \tag{3.11}$$

where

$$J_2(\sigma) = \frac{3}{2}\mathrm{s} : \mathrm{s} = \frac{1}{2}\left[(\sigma_{11}-\sigma_{22})^2 + (\sigma_{22}-\sigma_{33})^2 + (\sigma_{33}-\sigma_{11})^2\right] + 3\left[\sigma_{12}^2 + \sigma_{23}^2 + \sigma_{31}^2\right]. \tag{3.12}$$

The von Mises yield criterion is well known and stated as:

$$\sigma_{\text{eq}} \leq \sigma_Y, \tag{3.13}$$

where σ_Y is the yield stress. Equation (3.12) defines a yield surface in the shape of a circular cylinder around the hydrostatic axis (principal stresses are equal) in a coordinate system of principal stresses σ_{I}, σ_{II} and σ_{III}. Figure 3.1 shows the graphical representation of the von Mises yield criterion. The intersection of the von Mises yield surface with the deviatoric plane (where the sum of principal stresses is zero) is in the form of a circle. For a point inside the von Mises surface, the material is in the elastic regime; when a point is on the von Mises surface, the material enters the plastic regime. An alternative to the von Mises yield function is the Tresca yield function which is represented by a hexagonal yield surface in the space of principal axes. The von Mises yield criterion is usually used because it is more suitable for numerical analysis. For more information about the von Mises yield criterion refer to [14, 15].

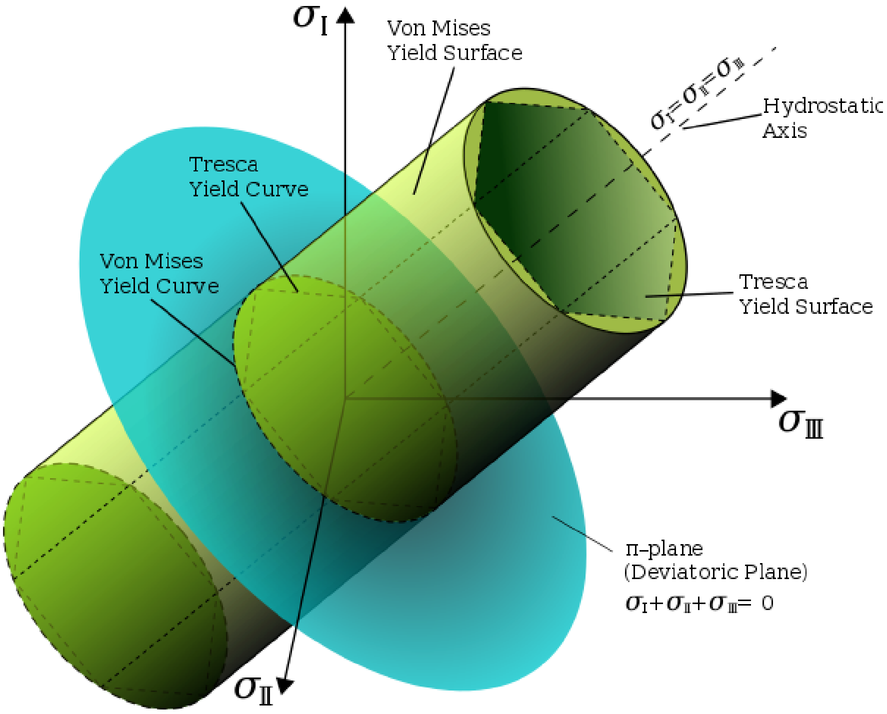

Figure 3.1: Von Mises yield surface [16]

The total strain is defined as:

$$\varepsilon^{\mathrm{tot}} = \varepsilon^{\mathrm{e}} + \varepsilon^{\mathrm{p}}. \tag{3.14}$$

The Cauchy stress is obtained through:

$$\sigma_{\mathrm{eq}} = \sigma_Y + R(p). \tag{3.15}$$

The $R(p)$ term represents the hardening stress and p is the plastic strain. The hardening stress can be described with an isotropic hardening model called power law [17]:

$$R(p) = kp^m, \tag{3.16}$$

where k and m are isotropic hardening parameters. For the power law, the parameters were obtained with linear regression using a rewritten form of (3.15) which is equivalent to the power law equation (3.16):

$$\underbrace{\sigma_{\text{eq}} - \sigma_Y}_{R(p)} = k(\underbrace{\varepsilon^{\text{tot}} - \frac{\sigma_Y}{E}}_{p})^m. \tag{3.17}$$

If we take the logarithms of equation (3.17)the following equation is obtained:

$$\log\left(\sigma_{\text{eq}} - \sigma_Y\right) = \log k + m \log\left(\varepsilon^{\text{tot}} - \frac{\sigma_Y}{E}\right), \tag{3.18}$$

where the values σ_{eq}, σ_Y, ε^{tot} and E are known and provided by the manufacturer through experimental data. The only unknown values are the strain hardening parameters k and m which can be easily obtained if there's a set of data, given the fact that they are parameters of a linear equation. Those parameters are shown in Chapter 6.

3.3.1 The Ramberg-Osgood equation

Equation (3.16) is, in fact, analogous of the well-known Ramberg-Osgood equation which is used for materials which exhibit hardening with plastic deformation. There is, although, a significant difference. The power law describes the strain hardening of the material in the plastic region and the relationship among stress and strain. The Ramberg-Osgood equation, on the other hand, is used for materials which exhibit an exponential relation between stress and strain both in the linear elastic and plastic region. It is assumed, that even in the linear elastic region, there are small permanent plastic deformations which are usually insignificant and thus neglected in the general case. The full Ramberg-Osgood equation found in [18] is:

$$\varepsilon = \frac{\sigma}{E} + \frac{\sigma^n}{F} = \varepsilon^{\text{e}} + \varepsilon^{\text{p}}, \tag{3.19}$$

where F is a proportionality constant and n is the strain hardening exponent.
It is also often written as:

$$\varepsilon = \frac{\sigma}{E} + K\left(\frac{\sigma}{E}\right)^n, \tag{3.20}$$

where K is the strain hardening modulus and n is the strain hardening exponent.

Furthermore, if a new parameter $\alpha = K\left(\sigma_0/E\right)^{n-1}$ is defined, where σ_0 is the yield strength, (3.20) can be rewritten as:

$$\varepsilon = \frac{\sigma}{E} + \alpha \frac{\sigma}{E}\left(\frac{\sigma}{\sigma_0}\right)^{n-1}, \tag{3.21}$$

which is yet another Ramberg-Osgood from used in Abaqus and described in [19].

The process of obtaining the strain hardening coefficient K and exponent n consists of plotting the stress-plastic strain curve in a log to log axis scale, where the curve becomes a straight line. Then the offset is equal to K and the slope to n. If the data doesn't fall on a straight line, then the Ramberg-Osgood equation is not suitable for that material.

For the material at hand, PBT Pocan B1305 000000, Figure 3.2 shows the plot of stress versus plastic strain in logarithmic scale.

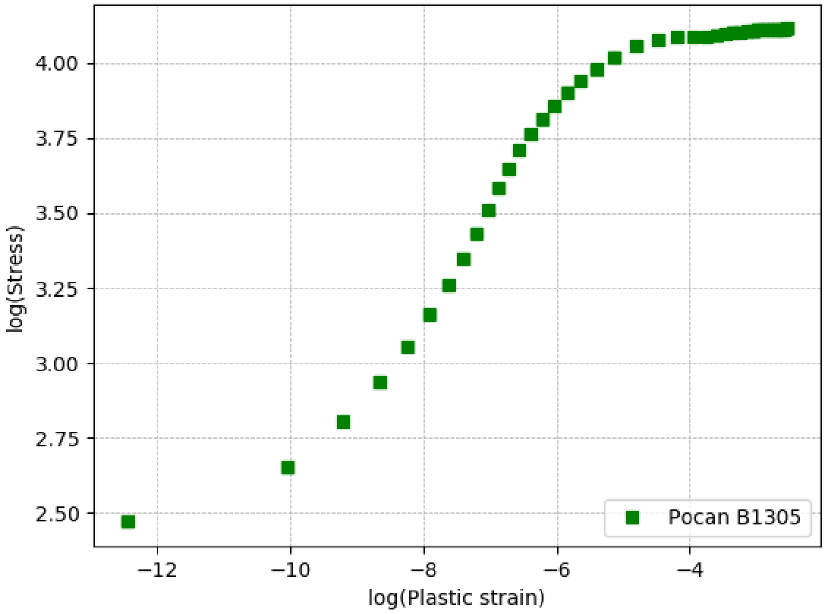

Figure 3.2: A plot of log(stress) versus log(plastic strain) for PBT Pocan B1305 000000

It can be clearly seen that the data does not fall on a straight line, therefore, it can be concluded that this material does not obey the Ramberg-Osgood law. Also, Figure 3.3 and Figure 3.4 show the same diagrams for Pocan B3225 and Pocan B3235.

An analogous conclusion can be made, i.e. those materials do not obey the Ramberg-Osgood law.

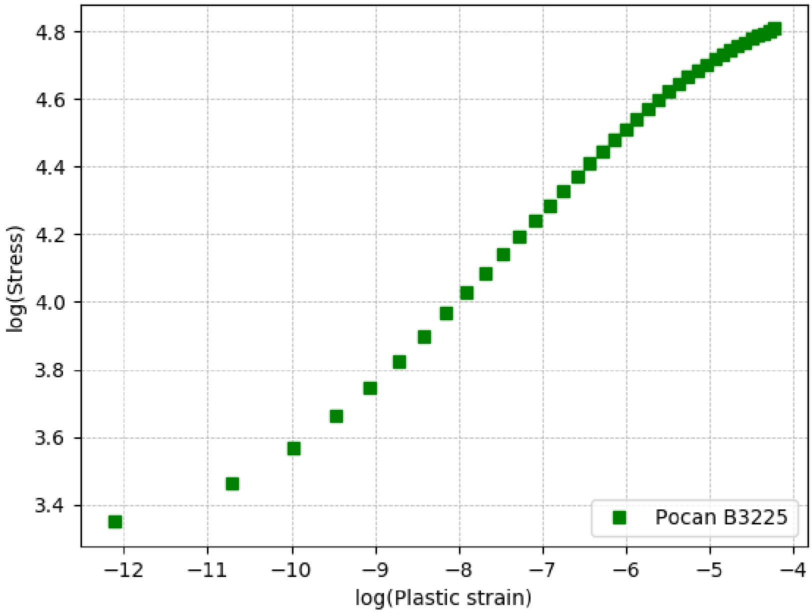

Figure 3.3: **A plot of log(stress) versus log(plastic strain) for PBT Pocan B3225 000000**

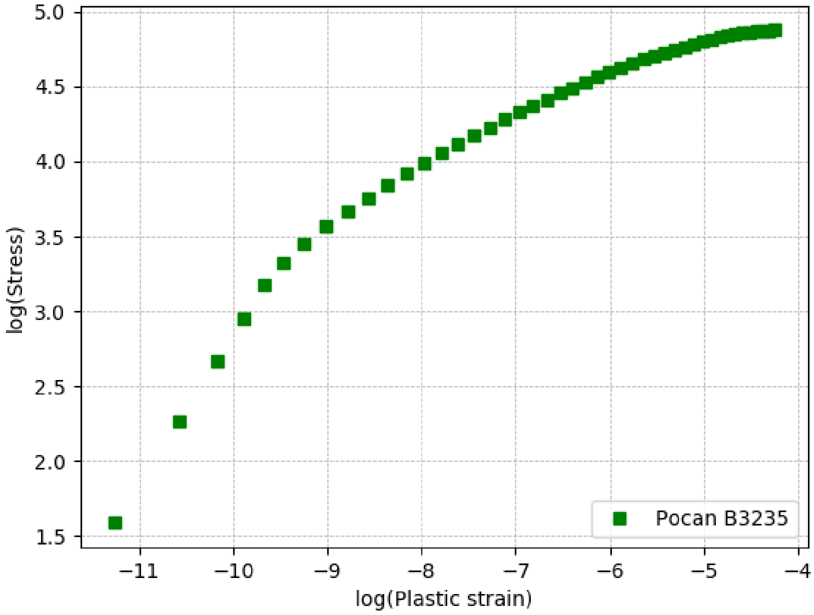

Figure 3.4: **A plot of log(stress) versus log(plastic strain) for PBT Pocan B3235 000000**

3.4 Summary

An insight into the concept of anisotropy is given. For the analysis, elasto-plastic material model will be used where the von Mises yield criterion is used. It was shown that the material PBT Pocan B1305 000000 does not obey the Ramberg-Osgood law, nor do its glass fiber reinforced variants.

4 Homogenization methods

4.1 Introduction

Fiber-reinforced composite materials are widely used in various industries. To model such materials, a micro-macro approach, which predicts the influence of the microstructure on the macroscopic properties was developed. The methods used in a micro-macro approach are known as homogenization methods. Homogenization methods are used to predict the response of heterogeneous materials, primarily composites, where the phases aside from the matrix can be inclusions, micro-cavities or micro-cracks. These methods are suitable for prediction of the response of thermoplastic polymers (PBT), which can be reinforced with glass fibers. If the properties of the phases and their volume fractions are known, a mean-field elasticity matrix which represents the homogenized material can be generated and used in further calculations while eliminating the need to measure the mechanical properties of the composite. The goal of homogenization is to reduce analysis time and memory use, with a reasonable accuracy.

Mean-field homogenization (MFH) provides the means for predicting the stresses and strains on the macro level with the use of the representative volume element (RVE), but it is not only limited to the macro level, meaning that the values for every phase in the composite can also be obtained [17]. A major role in this formulation is played by the concentration tensors that connect averaged fields in reinforcements or the matrix with the corresponding macroscopic fields [20]. In MFH, the inclusions must be made of the same material and have the same shape and orientation. This, in reality, is not the case, and the predictions may not always be completely accurate.

To obtain the most accurate predictions of micro stresses and strains in the phases, the direct finite element analysis (FEA) is used. Unfortunately, FEA has some drawbacks. For realistic micro-structures, complications arise during mesh generation. Furthermore, such analyses are very resource heavy and time consuming, especially for nonlinear problems. The main advantages of mean-field (MF) approaches are lower computational cost compared to the direct FEA approach, ease of use and low memory requirements.

The key parameters that have to be taken into account during the process of homogenization are the volume fraction and shape of the phases and their spatial distribution.

Homogenization methods provide very accurate predictions for the thermo-elastic properties of linear composites, although the use of these methods in the plastic regime may not always yield accurate results [21]. But, the high computational cost and the complexity of a direct finite element analysis of materials with high volume fractions and aspect ratios of inclusions are in favor of homogenization methods, such as the Mori-Tanaka method [20]. Figure 4.1 shows a representative microstructure sample with fibers and pores which can be homogenized.

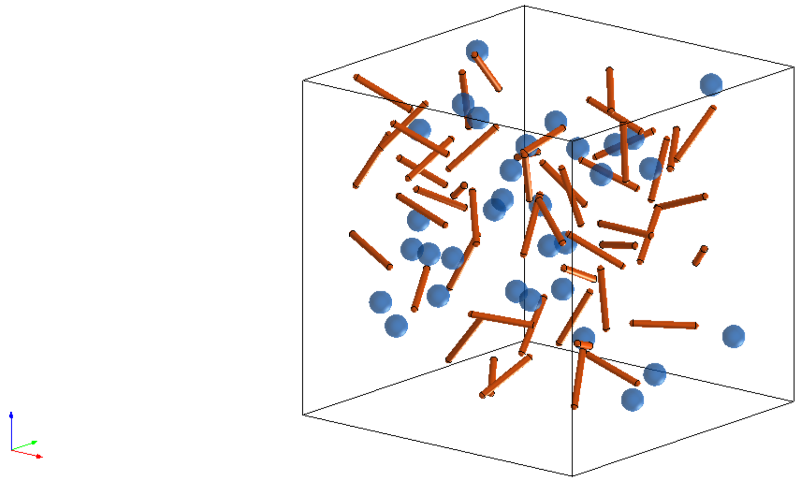

Figure 4.1: The microstructure of a composite material comprised of a matrix and inclusions, with pores present

4.2 The scope of mean-field homogenization

Homogenization methods are based on an analytical approach. They are used if the material is not locally homogeneous. In that case, the microscopic and macroscopic level have to be distinguished. The link between those two levels is the representative volume element (RVE), which has to be large enough to represent the heterogeneous microstructure while being as small as possible when compared with the solid body. With the RVE only a small sample of the material is observed to predict the microscopic response. Once the homogenized response of the composite is obtained, the macro constitutive equation is used for the prediction of material behavior, while the high computational cost is eliminated [17, 22].

The main objective of mean-field homogenization is to find the relationship between the volume averages of stress $\langle \boldsymbol{\sigma} \rangle_\omega$ and strain $\langle \boldsymbol{\varepsilon} \rangle_\omega$ over a RVE occupying a domain ω.

The simplest case where homogenization can be used is for a single inclusion problem which is based on Eshelby's solution [23]. For two-phase composites, homogenization methods based on single inclusion solution are used. For multi-phase composites, a two-step homogenization is usually carried out where the RVE is decomposed into homogenized pseudo-grains and homogenized over all pseudo grains [24, 25].

4.2.1 The representative volume element

The representative volume element (RVE) represents a small volume of the material on the microscopic level which is representative of the entire material. The RVE maps a heterogeneous medium to an equivalent homogeneous medium with average properties of the heterogeneous nonlinear material via homogenization. Although the RVE can be defined as 3D and 2D, the 3D RVE will be primarily used in this thesis because the 2D finite element models give invalid predictions compated to those obtained by 3D models [20]. Figure 4.1 shows a RVE with sphero-cylindrical inclusions and pores.

The RVE is primarily restricted by size in a sense that increasing its size results in problems with microstructure generation and meshing of the RVE as it can easily exceed the computational capabilities of modern day computers. In terms of generation of an acceptable mesh, the distance between inclusions also plays a significant role. Two important factors in RVE generation are the number and positioning of inclusions. "The number of inclusions is considered statistically representative if the composite response is unchanged when the number of inclusions is raised further at constant volume fraction", [22].

The orientation and length of inclusions present in the RVE can be obtained during the injection molding process with the use of software that can predict the second-rank orientation tensor, which replaces the orientation distribution function (ODF). The reason for this is that it is very hard to predict the ODF. For further elaboration on the concept of RVE see [26].

4.2.2 Periodic boundary conditions

To accurately fill the RVE with the desired volume of inclusions, periodic boundary conditions are introduced and the RVE must satisfy the periodicity criterion. The periodicity criterion ensures that the prescribed displacement remains conserved in all three directions. If the inclusion is cut on one boundary side of the RVE, the cut part has to be present on the opposite side of the RVE. If two separate RVE cubes were put together side by side, there would be no discontinuity in the constructed sample and all particles would have equal geometries [20]. This means that mesh compatibility is preserved and that it can be assumed that the RVE is infinite. As a consequence, the periodic boundary conditions make it possible to simulate an entire system by only simulating a small part. The periodic boundary conditions are governed with the following equation [21]:

$$\begin{aligned} \boldsymbol{u}(x,y,0) - \boldsymbol{u}_z &= \boldsymbol{u}(x,y,L) \\ \boldsymbol{u}(x,0,z) - \boldsymbol{u}_y &= \boldsymbol{u}(x,L,z) \quad . \\ \boldsymbol{u}(0,y,z) - \boldsymbol{u}_x &= \boldsymbol{u}(\alpha L,y,z) \end{aligned} \tag{4.1}$$

In (4.1) $\boldsymbol{u}$ is the displacement vector in the different faces of a quadrilateral prism and the vectors $\boldsymbol{u}_x$, $\boldsymbol{u}_y$ and $\boldsymbol{u}_z$ are the result of the loading on the RVE. The displacement vector is obtained when macro strain is applied to the RVE boundary. Figure 4.2 shows an illustration of periodic unit cells (RVEs). Periodic boundary conditions also contribute to reduction in computation time and better predictions of effective properties of heterogeneous materials.

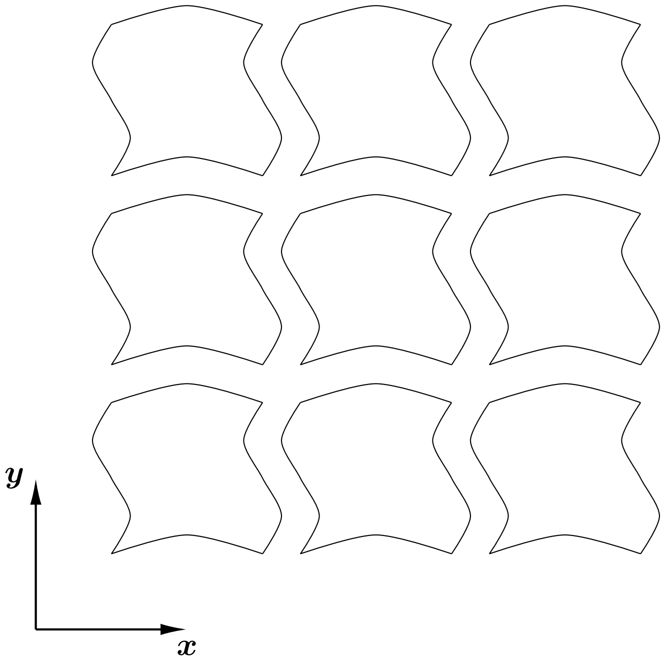

Figure 4.2: An illustration of periodic unit cells

4.2.3 The macro constitutive relation

If we have a body, and choose an arbitrary point $\mathbf{X}$ of that body, for a known macro strain $\boldsymbol{\varepsilon}(\mathbf{X})$ we can obtain the corresponding macro stress $\boldsymbol{\sigma}(\mathbf{X})$ and vice-versa. The average value over the domain ω of a volume V can be defined as:

$$\langle f(\mathbf{X},\mathbf{x})\rangle \equiv \frac{1}{V}\int_{\omega} f(\mathbf{X},\mathbf{x})\mathrm{d}V, \tag{4.2}$$

where $f(\mathbf{X}, \mathbf{x})$ represents the micro field in the RVE. If the relation between the macro values of stress $\boldsymbol{\sigma}(\mathbf{X})$ and strain $\boldsymbol{\varepsilon}(\mathbf{X})$ is found, this means that the average values of stress $\langle\boldsymbol{\sigma}\rangle_{\omega}$ and strain $\langle\boldsymbol{\varepsilon}\rangle_{\omega}$ are known because those values are equal [17, 27]. Therefore, the problem reduces to finding the macro stiffness $\overline{\mathbf{C}}$ shown in (4.3) and in Figure 4.3.

$$\langle\boldsymbol{\sigma}\rangle = \overline{\mathbf{C}} : \langle\boldsymbol{\varepsilon}\rangle \tag{4.3}$$

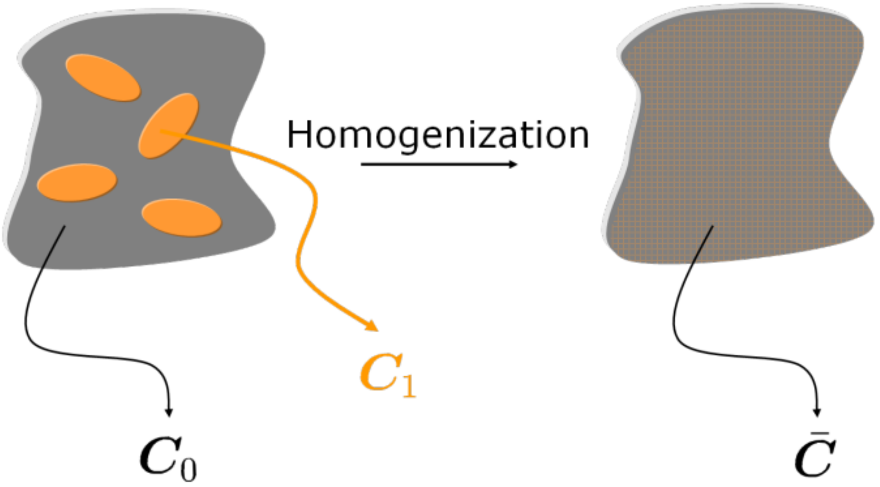

Figure 4.3: Depiction of macro stiffness [17]

Before the foundation for homogenization of two-phase composites is laid out, an overview of Eshelby's solution and the single inclusion problem will be presented.

4.2.4 Eshelby's solution

Eshelby's solution [23] serves as the cornerstone for the single inclusion problem and for two-phase homogenization. The assumption is that there's an infinite solid body with uniform stiffness C_0. If an ellipsoidal volume (I) of the body is cut out, subjected to a stress-free eigenstrain (radial expansion) ε^*, and then placed into the volume of the solid body it occupied, the strain that occurs in that ellipsoidal volume will be in relation with the stress-free eigenstrain. The occurring strain is uniform and linked with the stress-free eigenstrain through (4.4) where $\zeta(I, \mathbf{C}_0)$ is the Eshelby's tensor. Eshelby's tensor depends on the shape of the ellipsoidal volume (I), its orientation and the uniform stress in the solid body C_0.

$$\varepsilon(\mathbf{x}) = \zeta(I, \mathbf{C}_0) : \varepsilon^*, \quad \forall\ \mathbf{x} \in (I). \tag{4.4}$$

A detailed overview of Eshelby's tensor can be found in [2, 21, 26]. For circular inclusions, Eshelby's tensor has the form which is only dependent on the Poisson's ratio found in [28].

4.2.5 The single inclusion problem

The single inclusion problem is formulated for an infinite solid body which consists of a matrix with uniform stiffness $\mathbf{C}_0$ and a single ellipsoidal inclusion (I) with uniform stiffness $\mathbf{C}_1$ and to which linear displacements are applied. Those displacements are in correlation with the uniform remote strain $\mathbf{E}$. The relation between the remote strain $\mathbf{E}$ and the strain inside the inclusion (I) is:

$$\boldsymbol{\varepsilon}(\mathbf{x}) = \mathbf{H}^{\varepsilon}(I, \mathbf{C}_0, \mathbf{C}_1) : \mathbf{E}, \quad \forall\ \mathbf{x} \in (I), \tag{4.5}$$

where the strain inside the inclusion $\boldsymbol{\varepsilon}(\mathbf{x})$ is uniform and H the single inclusion strain concentration tensor [27]:

$$\mathbf{H}^{\varepsilon}(I, \mathbf{C}_0, \mathbf{C}_1) = \left\{\mathbf{I} + \zeta(I, \mathbf{C}_0) : \mathbf{C}_0^{-1} : [\mathbf{C}_1 - \mathbf{C}_0]\right\}^{-1}. \tag{4.6}$$

The single inclusion problem has an analytical solution and is therefore used as a basis for multi-inclusion problems which are based on a semi-analytical approach.

4.2.6 Two-phase composites

The assumption is that we have a two-phase composite, made of a matrix reinforced with multiple identical inclusions (same material, shape and orientation). To calculate the volume averages of strains in the RVE the following equation is used:

$$\langle\boldsymbol{\varepsilon}\rangle_{\omega} = \nu_0\langle\boldsymbol{\varepsilon}\rangle_{\omega_0} + \nu_1\langle\boldsymbol{\varepsilon}\rangle_{\omega_1}, \tag{4.7}$$

where the subscript 0 and 1 represent the volume average strain values associated with the matrix and the inclusions phase.

The following equation (4.8) describes the relation of strains in the inclusions ($\langle \boldsymbol{\varepsilon} \rangle_{\omega_1}$) with the strains in the matrix ($\langle \boldsymbol{\varepsilon} \rangle_{\omega_0}$) and the average macro strain in the composite ($\langle \boldsymbol{\varepsilon} \rangle_{\omega}$) through the strain concentration tensors $\mathbf{B}^{\varepsilon}$ and $\mathbf{A}^{\varepsilon}$ respectively:

$$\langle \boldsymbol{\varepsilon} \rangle_{\omega_1} = \mathbf{B}^{\varepsilon} : \langle \boldsymbol{\varepsilon} \rangle_{\omega_0} = \mathbf{A}^{\varepsilon} : \langle \boldsymbol{\varepsilon} \rangle_{\omega}, \tag{4.8}$$

where the relation between the strain concentration tensors $\mathbf{B}^{\varepsilon}$ and $\mathbf{A}^{\varepsilon}$ can be expressed as [22]:

$$\mathbf{A}^{\varepsilon} = \mathbf{B}^{\varepsilon} : \left[(1 - \nu_0) \, \mathbf{B}^{\varepsilon} + \nu_0 \mathbf{I} \right]^{-1}. \tag{4.9}$$

The average strains of the matrix and inclusion related to the average macro strain can the be written as:

$$\begin{aligned} \langle \boldsymbol{\varepsilon} \rangle_{\omega_0} &= \left[(1 - \nu_0) \, \mathbf{B}^{\varepsilon} + \nu_0 \mathbf{I} \right]^{-1} : \langle \boldsymbol{\varepsilon} \rangle \\ \langle \boldsymbol{\varepsilon} \rangle_{\omega_1} &= \mathbf{B}^{\varepsilon} : \left[(1 - \nu_0) \, \mathbf{B}^{\varepsilon} + \nu_0 \mathbf{I} \right]^{-1} : \langle \boldsymbol{\varepsilon} \rangle \end{aligned} \tag{4.10}$$

The domain ω represents the average values of strain, ω_0 the strain value in the matrix, and ω_1 the strain value in the inclusion. $\mathbf{I}$ represents the fourth-rank symmetric identity tensor. The macro stiffness is defined as:

$$\overline{\mathbf{C}} = \left[\nu_1 \mathbf{C}_1 : \mathbf{B}^{\varepsilon} + (1 - \nu_1) \, \mathbf{C}_0 \right] : \left[\nu_1 \mathbf{B}^{\varepsilon} + (1 - \nu_1) \, \mathbf{I} \right]^{-1}. \tag{4.11}$$

For the next step, the boundary conditions have to be defined. Displacement boundary conditions are applied as:

$$\boldsymbol{u}(\boldsymbol{x}) = \boldsymbol{\varepsilon}^{\infty} \cdot \boldsymbol{x} \quad \forall \boldsymbol{x} \in \partial \omega^*. \tag{4.12}$$

ω^* is the domain of the isolated inclusion cell and $\boldsymbol{\varepsilon}^{\infty}$ is the far-field strain.

To obtain the average strain of all inclusions, the inclusions are replaced with an equivalent single inclusion. This is known as the equivalent inclusion problem (EIP). To obtain the displacement field the following boundary value problem has to be solved:

$$\begin{cases} \operatorname{div}(\boldsymbol{\sigma}) = 0, \quad \forall \boldsymbol{x} \in \omega^* \\ \boldsymbol{u}(\boldsymbol{x}) = \boldsymbol{\varepsilon}^{\infty} \cdot \boldsymbol{x} \quad \forall \boldsymbol{x} \in \partial\omega^* \\ \boldsymbol{\varepsilon}(\boldsymbol{x}) = \frac{1}{2}\left(\nabla \boldsymbol{u}(\boldsymbol{x}) + \nabla^T \boldsymbol{u}(\boldsymbol{x})\right) \\ \text{(constitutive equations)} \end{cases} \tag{4.13}$$

The matrix average strain is unknown, so iterations over the values of $\langle\boldsymbol{\varepsilon}\rangle_{\omega_0}$ must be carried out, each of them requiring the FE resolution of the EIP and leading to an updated value of $\langle\boldsymbol{\varepsilon}\rangle_{\omega_1}$, until (4.7) is satisfied.

Once the phase strains are known, the average stress in each phase can be calculated. The macroscopic stress is defined as the stress average over the composite:

$$\langle\boldsymbol{\sigma}\rangle \equiv \nu_0\langle\boldsymbol{\sigma}\rangle_{\omega_0} + \nu_1\langle\boldsymbol{\sigma}\rangle_{\omega_1}. \tag{4.14}$$

For a further reference on this problem, see [29].

4.2.7 Multi-phase composites

In contrary to two-phase composites, which have only one inclusion phase, multi-phase composites may have two or more inclusions phases. The inclusion phases can be made of different materials, with different shapes and orientations. Therefore, for multi-phase composites, the multi-level method is used [17]. At each level, a similar procedure as for two-phase composites is used. The first set of inclusions is homogenized with the matrix on the deepest level, usually by using the Mori-Tanaka method. This new homogenized medium assumes the role of a matrix for the next level where it is further homogenized with that level's set of inclusions. This procedure repeats until all the inclusion sets have been homogenized and we have one homogenized medium.

The order of inclusion sets to be homogenized at each level has to be accounted for because it may result in poor predictions. Currently, it is recommended to to add the inclusions sets with the lowest rigidity first [17].

4.2.8 Numerical procedure

To initialize the numerical procedure it is assumed that the average strain in the matrix equals the macroscopic strain:

$$\langle \boldsymbol{\varepsilon} \rangle_{\omega_0} \leftarrow \langle \boldsymbol{\varepsilon} \rangle \tag{4.15}$$

Iteration is carried out in the following steps and can be found in [22], p. 720.

1. Apply displacement boundary conditions (4.13) to the EIP.

2. Solve the EIP by the FE method for the considered time increment, starting from the deformed state at t_n.

3. Compute the average strain in the inclusions of the actual composite as:

$$\langle \boldsymbol{\varepsilon} \rangle_{\omega_1} = \langle \boldsymbol{\varepsilon} \rangle_{\omega_1^*} = \frac{1}{V\left(\omega_1^*\right)} \sum_{k=1}^{N_k} \boldsymbol{\varepsilon}_k V_k \tag{4.16}$$

   where $\boldsymbol{\varepsilon}_k$ is the strain at the integration point k; V_k is the volume associated with the integration point k, and N_k the total number of integration points in the discretized domain ω_1^*

4. Check compatibility of average strain in the inclusions by computing residual:

$$\boldsymbol{R} = \frac{\langle \boldsymbol{\varepsilon} \rangle - \nu_1 \langle \boldsymbol{\varepsilon} \rangle_{\omega_1}}{\nu_0} - \langle \boldsymbol{\varepsilon} \rangle_{\omega_0} \tag{4.17}$$

5. If $|\boldsymbol{R}| < \mathrm{TOL}$ then exit the loop.

6. Else: new iteration with new $\langle \boldsymbol{\varepsilon} \rangle_{\omega_0}$.

$$\langle \boldsymbol{\varepsilon} \rangle_{\omega_0} \leftarrow \langle \boldsymbol{\varepsilon} \rangle_{\omega_0} + \boldsymbol{R} \tag{4.18}$$

After convergence, the average matrix stress $\langle \boldsymbol{\sigma} \rangle_{\omega_0}$ is approximated by calling the constitutive box with the average strain $\langle \boldsymbol{\varepsilon} \rangle_{\omega_0}$, average strain increment $\langle \Delta\boldsymbol{\varepsilon} \rangle_{\omega_0}$ and the history variables at t_n. The macroscopic stress can then be calculated using (4.14). This procedure is also described in [27, 29].

4.2.9 Nonlinear inelastic materials

If two-phase composite materials made of elasto-plastic phases are considered, a tangent operator based on incremental formulation is used to relate the phase stresses and strains and linearize the response. The relation can be stated as:

$$\dot{\boldsymbol{\sigma}}(\mathbf{x},t) = \mathbf{C}_r(\boldsymbol{\varepsilon}(\mathbf{x},t),t) : \dot{\boldsymbol{\varepsilon}}(\mathbf{x},t), \qquad \forall \ \mathbf{x} \in \omega_r, \quad r = 0, 1, \tag{4.19}$$

where $r = 0, 1$ denotes either the matrix phase or the inclusion phase as stated before. The relation is comparable to linear elasticity where instead of stress and strain we have stress and strain rates, while Hooke's elastic stiffness tensor is replaced with the tangent operator. The difference is that the operator relating the stress and strain rates is no longer uniform per phase.

But, one issue arises with this approach if an elasto-plastic matrix reinforced with stiffer elastic inclusions is considered. If this approach is used, the predicted response will be as in Figure 4.4. It can be seen that the predictions marked as plus and cross signs are stiffer than the FE results. This issue arises because the incremental formulation is based on anisotropic tangent operators (continuum and consistent tangent operators), but if only the isotropic part of tangent operators is used, better results can be obtained which are marked with star signs.

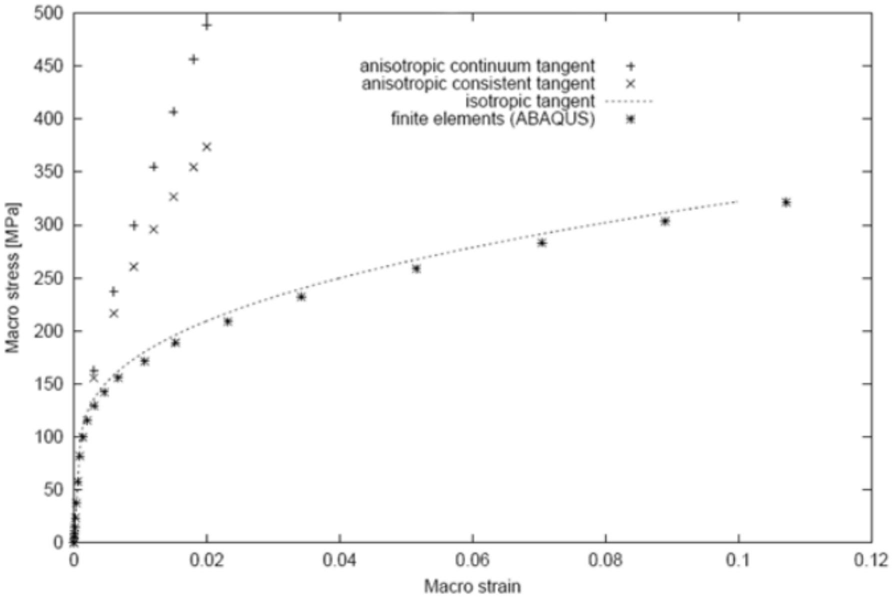

Figure 4.4: Comparison of the stress-strain predictions for an elasto-plastic matrix with stiffer inclusions [29]

Here, the main focus will be on the J_2 elasto-plasticity which is covered in more detail in [29]. The continuum tangent operator for elasto-plasticity with J_2 flow theory and isotropic hardening is can be stated as:

$$\mathbf{C}^{\mathrm{ep}} = \mathbf{C}^{\mathrm{el}} - \frac{(2G)^2}{h}\mathbf{N} \otimes \mathbf{N}, \quad \mathbf{N} = \frac{\partial f}{\partial \boldsymbol{\sigma}} = \frac{3}{2}\frac{\operatorname{dev}(\boldsymbol{\sigma})}{\sigma_{eq}}, \quad h = 3G + \frac{\mathrm{d}R}{\mathrm{d}p}. \tag{4.20}$$

As it was described earlier, p is the accumulated plastic strain and $R(p)$ the hardening stress. $\mathbf{N}$ represents the normal to the yield surface in stress space. An algorithmic tangent operator for numerical procedure can be defined after discretizing the equation with the implicit backward Euler scheme. The discretized equation is then linearized:

$$\mathbf{C}^{\mathrm{alg}} = \mathbf{C}^{\mathrm{ep}} - (2G)^2 \Delta p \frac{\sigma_{\mathrm{eq}}}{\sigma_{\mathrm{eq}}^{\mathrm{tr}}}\frac{\partial \mathbf{N}}{\partial \boldsymbol{\sigma}}, \quad \frac{\partial \mathbf{N}}{\partial \boldsymbol{\sigma}} = \frac{1}{\sigma_{\mathrm{eq}}}\left(\frac{3}{2}\mathbf{I}^{\mathrm{dev}} - \mathbf{N} \otimes \mathbf{N}\right), \tag{4.21}$$

where $\sigma_{\mathrm{eq}}^{\mathrm{tr}}$ is the elastic predictor (denotes the trial value for the iterative procedure, usually obtained from the assumption that, initially, the stiffness tensor is elastic, hence the name elastic predictor). The obtained consistent tangent operator is used to describe the relation of stress and strain after each time increment. It is clear that, if Δp reaches zero, $\mathbf{C}^{alg} = \mathbf{C}^{ep}$. As we have seen the tangent operators are not isotropic, so isotropization has to be carried out by applying either the spectral or general isotropization method [29].

4.3 Mori-Tanaka model

The Mori-Tanaka model was introduced by Mori and Tanaka in 1973 [30]. It is obtained through the derivation of Eshelby's solution. It is based on the assumption of an infinite body subjected to the average matrix strain equal to the far field strain [17, 22, 31, 32]. For this model, the strain concentration is:

$$\mathbf{B}^{\varepsilon} = \mathbf{H}^{\varepsilon}\left(I, \mathbf{C}_0, \mathbf{C}_1\right) \tag{4.22}$$

where the operator $\mathbf{H}^{\varepsilon}$ is the operator for the single inclusion problem [27]. The behavior of every inclusion in the RVE is described with the behavior of one equivalent single inclusion present in the matrix as seen in Figure 4.5. The Mori-Tanaka's tensor can be found in [2].

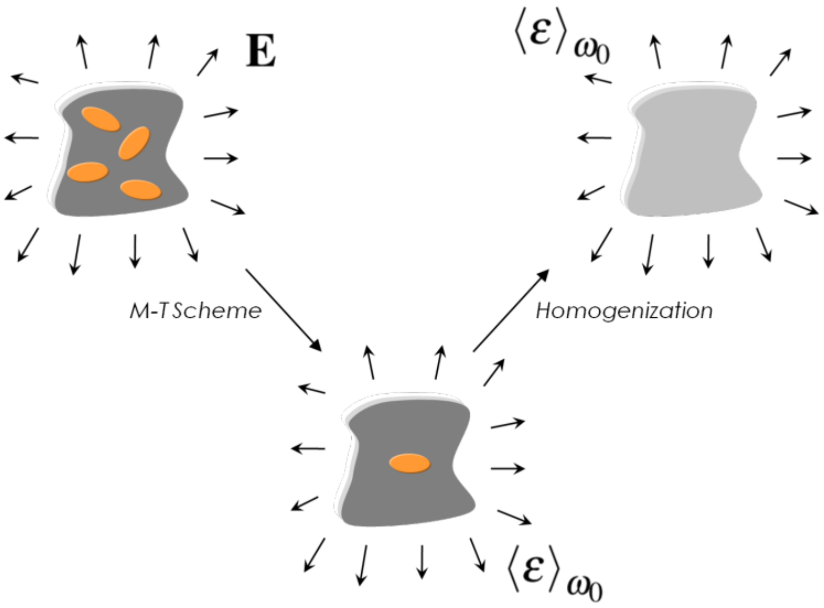

Figure 4.5: Mori-Tanaka Model [17]

The Mori-Tanaka formulation yields a symmetric stiffness tensor only if all the inclusions have the same aspect ratio and orientation. Furthermore, to obtain valid results, the inclusions must have identical aspect ratios and be all equally aligned [2, 24, 32, 33].

The Mori-Tanaka method can be used for the modeling of two-phase elasto-plastic composites for low to moderate volume fractions of inclusions. Other semi-analytical schemes based on the M-T method should yield valid predictions. The Mori-Tanaka method can be extended to model inhomogenieties of non-ellipsoidal shapes by defining replacement stiffness tensors [28].

A further extension of the Mori-Tanaka model was made with the incremental approach. In this approach, the MT model is employed at the element Gauss points as a micromechanical constitutive model that describes the effective (macroscopic) response of a heterogeneous material. Different approaches on the incremental Mori-Tanaka method can be found in [29, 34], where the latter, AD-based formulation of the MT scheme, shows a improved efficiency and drastically reduces the computation time.

4.3.1 Limitations of the Mori-Tanaka method

The Mori-Tanaka model can accurately predict the properties for two-phase composites with the volume fractions of inclusions lower than 25 percent, but it gives good predictions even beyond this range. The predictions of phase averages are accurate for volume fractions below 15 percent. The poor predictions for composites with the volume fraction of inclusions above 25 percent is a consequence of plastic localization which occurs between inclusions of the composite, which is not taken into account by the MF model. If the inclusions aren't identical, the results may be invalid [17, 22].

4.4 Summary

Homogenization was described and its application was shown. The concept of a RVE was introduced and the periodic boundary conditions were discussed. An overview of Eshelby's solution and the single inclusion problem was shown. After that, homogenization of two-phase composites was described. Finally, the Mori-Tanaka model was shown.

The homogenization approach simplifies the modeling of nonlinearity in the material. However, caution is advised because in some cases (short fiber reinforced thermoplastic polymers), the predictions may differ with FE results or experimental results. If this is the case, second-order MFH can provide better results [17]. More recent studies in the field of porous plasticity in regards of macroscopic yielding and plastic behavior of isotropic porous materials with spherical pores are discussed in [35, 36, 37].

5 The finite element method

5.1 Introduction and overview

The finite element method is a method developed to model and predict the responses of various systems. This ranges from structural analyses to computational fluid dynamics problems. It is primarily used in structural analyses. The principle the method is based on assumes that a body can be modeled by discretizing it to smaller parts, thus reducing an infinite number of degrees of freedom to a finite number of degrees of freedom. With the increase of number of elements, we can obtain a closer representation of the real behavior, but this comes at a cost, namely the computation time is longer. The finite element method gained traction with the development of more sophisticated computer systems and is one of the predominant methods for problem solving in the area of mechanical engineering. For a more detailed overview refer to [12, 14, 38].

5.2 Element types

Various types of elements have been developed for many different applications. One-dimensional, two-dimensional and three-dimensional elements are distinguished. If the geometry can be simplified, the use of 1D and 2D elements is recommended, thus greatly reducing the computation time because in this case we are dealing with a simpler model and the number of elements is greatly reduced. The FE analyses of RVEs are carried out in Abaqus, and the element types used are from Abaqus element library. Second-order elements are used.

For the analysis of a RVE, 2D and 3D elements are used. 2D models are discretized with 6-node triangular elements (CPE6) which have 2 degrees of freedom in every node. The element CPE6 has 3 integration points. The displacement vector is described by a second-order polynomial:

$$\begin{bmatrix} u \\ v \end{bmatrix} = \begin{bmatrix} 1 & x & y & x^2 & xy & y^2 & 0 & 0 & 0 & 0 & 0 & 0 \\ 0 & 0 & 0 & 0 & 0 & 0 & 1 & x & y & x^2 & xy & y^2 \end{bmatrix} \begin{bmatrix} a_1 \\ a_1 \\ . \\ a_{12} \end{bmatrix} \tag{5.1}$$

For simplicity, (5.1) is rewritten in matrix form:

$$\mathbf{u} = \boldsymbol{\alpha}\mathbf{a}. \tag{5.2}$$

From that, the matrix of shape functions which correlates the displacement vector **u** and the vector of nodal displacements **v** can be found:

$$\mathbf{u} = \mathbf{N}\mathbf{v}. \tag{5.3}$$

The stress and strain distribution in this element is linear. The element can be seen in Figure 5.1.

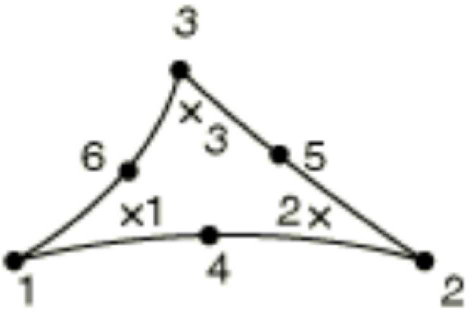

Figure 5.1: The 6-node triangular element (CPE6) [19]

For the 3D models, two types of elements are used. For the 3D RVE, 10-node tetrahedron elements (C3D10), which can be seen in Figure 5.2, are used. This element type has 10 nodes with a total of 30 degrees of freedom. The displacement vector is also described by a second-order polynomial in the following form:

$$\begin{bmatrix} u \\ v \\ w \end{bmatrix} = \begin{bmatrix} p & 0 & 0 & 0 & 0 & 0 & 0 & 0 & 0 & 0 & 0 & 0 & 0 & 0 & 0 & 0 & 0 & 0 & 0 & 0 & 0 \\ 0 & 0 & 0 & 0 & 0 & 0 & 0 & 0 & 0 & 0 & p & 0 & 0 & 0 & 0 & 0 & 0 & 0 & 0 & 0 & 0 \\ 0 & 0 & 0 & 0 & 0 & 0 & 0 & 0 & 0 & 0 & 0 & 0 & 0 & 0 & 0 & 0 & 0 & 0 & 0 & 0 & p \end{bmatrix} \begin{bmatrix} a_1 \\ a_1 \\ . \\ a_{30} \end{bmatrix},$$

$$p = \begin{bmatrix} 1 & x & y & z & x^2 & y^2 & z^2 & xy & yz & xz \end{bmatrix} \tag{5.4}$$

Shape functions can be obtained similarly to the procedure described for the CPE6 element. This element also has a linear stress and strain distribution. Furthermore, a variant of this element labeled as C3D10M which has hourglass control, is used to prevent volumetric locking. The C3D10M element type uses a modified second-order interpolation.

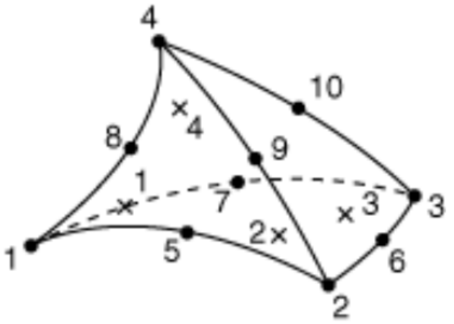

Figure 5.2: The 10-node tetrahedron element (C3D10) [19]

For the tension specimen, a 20-node brick element with reduced integration (C3D20R) is used (Figure 5.3). Reduced integration is used for non-linear problems to reduce the stiffness of the element and computation time. This element only has nodes distributed along its edges. Each node has 3 degrees of freedom for a total of 60 degrees of freedom. More about the elements used can be found in Abaqus Analysis User's Guide [19].

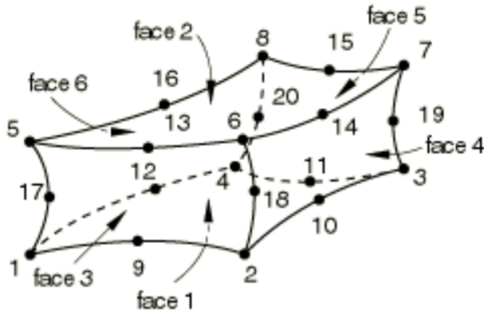

Figure 5.3: The 20-node brick element (C3D20R) [19]

5.3 Summary

An overview of the finite element method is given and the elements used are shown. Basic characteristics of used elements are described. For the 2D analysis plane strain elements are used (CPE6) and for 3D analysis solid elements are used (C3D10, C3D10M, C3D20R). The C3D10M elements will be used for discretization of a 3D RVE and the C3D20R elements for discretization of a tension specimen.

6 Mechanical behavior of PBT resin - analysis and results

6.1 Introduction

The first step is to verify the elasticity matrix. A comparison of the analytically obtained elasticity matrix, an elasticity matrix generated by Digimat MF and a matrix obtained through a strain perturbation technique, is made. Afterwards, different approaches are taken in the modeling of the constitutive response of PBT.

The first approach includes the testing of the material response by the use of a RVE. Samples of different microstructures are generated and tested to obtain the volume average response of the material. The intention is to use the homogenized properties for different sets of pore volume fractions and show that the stress fields are indeed dependent on the heterogeneity of the material. With the rise of pore volume fraction we expect the stiffness of models to drop for the same loading and boundary conditions.

After that, a model of a tension specimen is created and tested under the appropriate loads and boundary conditions. This approach uses a UMAT subroutine through the Digimat CAE interface, where in every iteration, homogenized fields are obtained with the use of the Mori-Tanaka method.

6.1.1 Prerequisites and assumptions

The microstructure of PBT where pores are present is modeled. The matrix (PBT) is modeled as an elasto-plastic material. With the standard Poisson's ratio and Young's modulus, the hardening parameters have to be defined. Pores are defined by the volume fraction and the average radius of pores. An idealization of shape is made and pores are modeled as spheres. Two types of analyses are carried out for the RVE. First, small strains are considered. After that, the large strain approach is taken. The obtained results are then compared. For small strains, the strain tensor has the following form:

$$\varepsilon_{ij} = \frac{1}{2}\left(u_{i,j} + u_{j,i}\right) = \begin{bmatrix} \frac{\partial u_1}{\partial x_1} & \frac{1}{2}\left(\frac{\partial u_1}{\partial x_2} + \frac{\partial u_2}{\partial x_1}\right) & \frac{1}{2}\left(\frac{\partial u_1}{\partial x_3} + \frac{\partial u_3}{\partial x_1}\right) \\ \frac{1}{2}\left(\frac{\partial u_2}{\partial x_1} + \frac{\partial u_1}{\partial x_2}\right) & \frac{\partial u_2}{\partial x_2} & \frac{1}{2}\left(\frac{\partial u_2}{\partial x_3} + \frac{\partial u_3}{\partial x_2}\right) \\ \frac{1}{2}\left(\frac{\partial u_3}{\partial x_1} + \frac{\partial u_1}{\partial x_3}\right) & \frac{1}{2}\left(\frac{\partial u_3}{\partial x_2} + \frac{\partial u_2}{\partial x_3}\right) & \frac{\partial u_3}{\partial x_3} \end{bmatrix} \tag{6.1}$$

When large strains are considered, the assumption that the undeformed and deformed configurations are equal is no longer valid. For large deformations, the deformed configuration exhibits geometric nonlinearity, and the equilibrium has to be defined for the deformed configuration. The finite strain tensor has the following form:

$$\varepsilon_{ij} = \frac{1}{2}\left(\frac{\partial u_i}{\partial x_j} + \frac{\partial u_j}{\partial x_i} - \frac{\partial u_k}{\partial x_i}\frac{\partial u_k}{\partial x_j}\right). \tag{6.2}$$

Compared to the infinitesimal strain tensor (6.1), the finite strain tensor has an additional term. When small strains are assumed, the last term of (6.2) vanishes and the infinitesimal strain tensor is obtained.

6.2 Elasticity matrix verification

Three methods are used to determine the elasticity matrix of PBT. An analytical solution is obtained by using equation (3.10). Following that, Digimat MF is used. Finally, a direct FE simulation where uniaxial loadings are applied as 100 percent of deformation for each component, thus obtaining a homogenized stress tensor which corresponds to a single row and column of an elasticity matrix. For the analytical solution, parameters $E = 2800$ MPa and $\nu = 0.3981$ are used. With substituting those parameters into (3.10), the following elasticity matrix is obtained:

$$\boldsymbol{C} = \begin{bmatrix} 5914.8 & 3912.1 & 3912.1 & 0 & 0 & 0 \\ 3912.1 & 5914.8 & 3912.1 & 0 & 0 & 0 \\ 3912.1 & 3912.1 & 5914.8 & 0 & 0 & 0 \\ 0 & 0 & 0 & 1001.4 & 0 & 0 \\ 0 & 0 & 0 & 0 & 1001.4 & 0 \\ 0 & 0 & 0 & 0 & 0 & 1001.4 \end{bmatrix} \tag{6.3}$$

With Digimat MF, the following stiffness matrix is obtained:

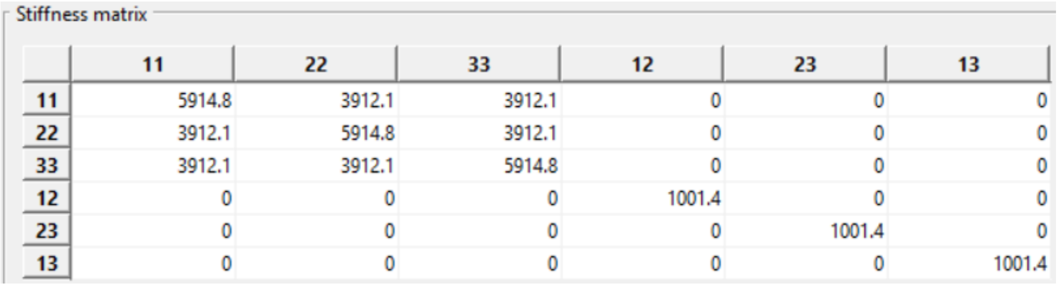

	11	22	33	12	23	13
11	5914.8	3912.1	3912.1	0	0	0
22	3912.1	5914.8	3912.1	0	0	0
33	3912.1	3912.1	5914.8	0	0	0
12	0	0	0	1001.4	0	0
23	0	0	0	0	1001.4	0
13	0	0	0	0	0	1001.4

Figure 6.1: Stiffness matrix of PBT obtained with Digimat MF

Finally, with a direct FE analysis, the same stiffness matrix is obtained. The stress values correspond to the elements of the elasticity matrix of PBT, namely: $C_{1111} = 5927.68$, $C_{1122} = 3922.08$, $C_{1133} = 3920.84$, $C_{1212} = 1003.56$. All other elements of the matrix are zero.

If the values obtained with those three methods are compared, it clearly shows that the same elasticity matrix is obtained (Table 6.1).

Table 6.1: Comparison of elasticity tensor components

\	C_{1111}	C_{1122}	C_{1133}	C_{1212}
Analytical	5914.8	3912.1	3912.1	1001.4
Digimat MF	5914.8	3912.1	3912.1	1001.4
Strain perturbation	5927.68	3922.08	3920.84	1003.56

6.3 RVE model

The representative volume element is used in this approach. RVE's are generated for different volume fractions of pores. Then a comparison is made to observe how the increasing of pores volume fraction affects the strength of PBT.

The generation of the representative volume element can be a challenging task, especially if random orientation is desired. Another constraint is imposed by the aspect ratio of inclusions. "Inclusions with an ellipsoidal shape and an aspect ratio larger than 10 can lead to errors during the automatic meshing" [17]. In such cases, the resulting geometry is very complex and can even be invalid, which invokes meshing difficulties. Therefore, it is necessary to repeat the representative volume element generation procedure until the random geometry becomes valid and does not cause meshing difficulties.

On a side note, caution is advised because the generated geometry is not always the same if random orientation is enabled. Even if the valid geometry criterion is satisfied, it may take a large number of finite elements to obtain accurate stress and strain results. Another option is to allow size reduction, which helps in geometry generation, with a drawback that this option causes difficulties with reaching reference volume fractions in the RVE.

The RVE's are discretized with tetrahedron elements labeled as C3D10M. This modified tetrahedron has hourglass control enabled and exhibits minimal volumetric locking during plastic straining, thus capturing the strain gradients in the matrix between the inclusions better than the standard 10-node tetrahedron because it has three extra internal degrees of freedom [21]. When combined with 3D orientation, parabolic elements can be very resource demanding, so it is better to do the testing with linear elements and only the final analysis with parabolic elements.

The whole process can be summed as:

1. Generate the geometry
2. Mesh the geometry
3. Carry out the FE analysis
4. Obtain the average values over stress and strain fields

6.3.1 Elasto-plastic model

First, an overview of true stress and true strain is shown. True stress and strain differ from engineering stress and strain in that, when calculating the true values, we assume that the section area changes, contrary to engineering values where we assume that the section area doesn't change and is constant throughout the whole loading regime. This can be summed by the following equations. Equation (6.4) shows the expressions for calculating the engineering values of stress and strain and (6.5) shows the same for true stress and strain:

$$S = \frac{F}{A_0} = \sigma_\epsilon, \qquad \varepsilon_\epsilon = \frac{l - l_0}{l_0} = \frac{\Delta l}{l_0}, \tag{6.4}$$

$$\sigma = \frac{F}{A}, \qquad \varepsilon = \int_{l_0}^{l} \frac{\mathrm{d}l}{l} = \ln\frac{l}{l_0}, \tag{6.5}$$

where A is the time-dependent section area which changes during loading, and A_0 is the initial section area. From (6.4) and (6.5) we can obtain the relation between the true and engineering values of stress and strain. We can observe that $\varepsilon_\epsilon = \frac{l}{l_0} - 1$; therefore, we can express the true strain as a function of engineering strain as:

$$\varepsilon = \ln\left(\varepsilon_\epsilon + 1\right) \tag{6.6}$$

From the fact that the volume has to be the same for both cases we have:

$$V_0 = A_0 l_0 = V = Al, \tag{6.7}$$

and then can obtain the relation of area ratio vs. length ratio:

$$\frac{A_0}{A} = \frac{l}{l_0} \tag{6.8}$$

If we define a ratio of true and engineering stress as:

$$\frac{\sigma}{S} = \frac{A_0}{A} = \frac{l}{l_0}, \tag{6.9}$$

then we can obtain the relation between those two values by substituting the expression $\varepsilon_\epsilon + 1$ instead of $\frac{l}{l_0}$ as shown before. Finally, we obtain the expression for the true stress as a function of engineering stress and engineering strain:

$$\sigma = S\left(\varepsilon_\epsilon + 1\right). \tag{6.10}$$

If we assume a material which has a stress strain curve as shown in Figure 6.2, we can calculate the plastic strain of any given data point. For a more accurate definition of plastic behavior, true stress and trues strain values can be used.

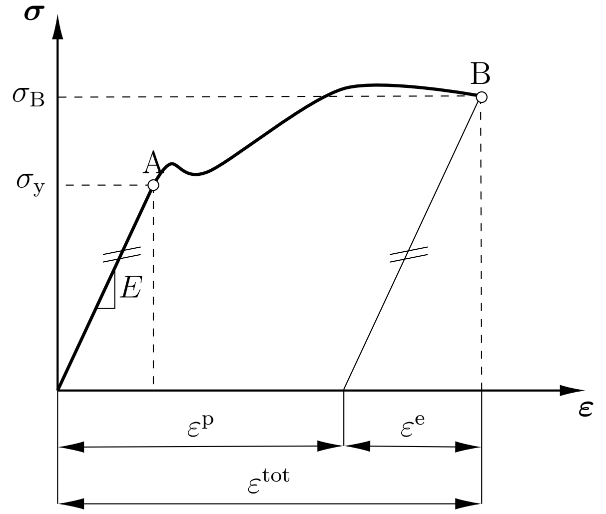

Figure 6.2: Elasto-plastic material model

With experimental data, we know the total strain and stress values at every measured point. For the relation for total strain see (3.14). To obtain the elastic strain for a measured strain value in the plastic region we need to know the true stress and Young's modulus E. For example, if we look at point B in Figure 6.2, the elastic strain can be obtained as:

$$\varepsilon^\mathrm{e} = \frac{\sigma_\mathrm{B}}{E}. \tag{6.11}$$

If we generalize (6.11), we can assume that it is valid for any measured total stress value. Therefore, we can write the expression for calculating the plastic strain from experimentally obtained true stress and true strain.

$$\varepsilon^\mathrm{p} = \varepsilon^\mathrm{tot} - \frac{\sigma}{E} \tag{6.12}$$

To define the elasto-plastic model, the data from [4] was used and can be seen in Table 6.2. The data was approximated by the power law. Prior to that, an approximation of the elastic line was created to determine the limit between the elastic and plastic region. It was determined that the limit is at strain value $\varepsilon = 2.0582$ % and stress value $\sigma = 49.459$ as shown in Figure 6.3. After that, linear regression was used in *Python* to determine the strain hardening parameters. The comparison of suppliers data and the approximation is shown in Figure 6.4.

Table 6.2: Stress-strain data for Pocan B1305 000000 at 23 °C

Strain, [%]	Stress, [MPa]	Strain, [%]	Stress, [MPa]
0	0	2.0582	49.459
0.0491	1.386	2.1971	51.5
0.0991	2.797	2.3625	53.574
0.1491	4.209	2.5798	55.726
0.1991	5.62	2.8773	57.751
0.2491	7.031	3.2531	59.12
0.3357	9.447	3.6592	59.608
0.423	11.833	4.0667	59.639
0.5114	14.198	4.4738	59.7
0.601	16.549	4.8807	59.858
0.6922	18.896	5.2877	60.073
0.7853	21.249	5.6948	60.309
0.8806	23.622	6.1019	60.526
0.9781	26.023	6.5093	60.695
1.0778	28.456	6.9169	60.817
1.1795	30.927	7.3246	60.904
1.2829	33.433	7.7325	60.966
1.3878	35.947	8.1404	61.014
1.494	38.427	8.5484	61.057
1.601	40.834	8.9566	61.098
1.7088	43.128	9.3647	61.136
1.819	45.309	9.773	61.174
1.9341	47.408	10.1813	61.21

Although the suppliers data shown in Table 2.1 states that the yield strength is 60 MPa, it was determined from Figure 6.3 that the elastic limit is at $\sigma_Y = 49.459$ MPa and this value was used to obtain the hardening parameters because it gives a better approximation of the given data.

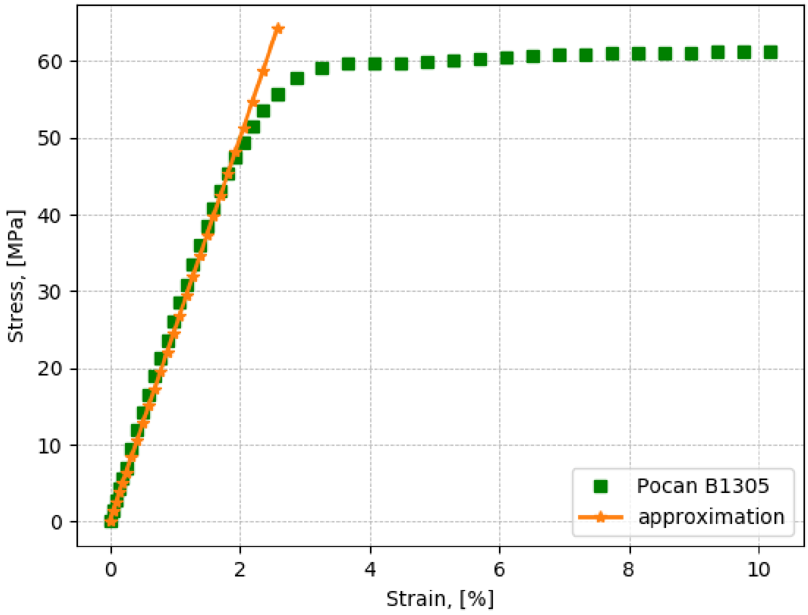

Figure 6.3: Approximation of the elastic region

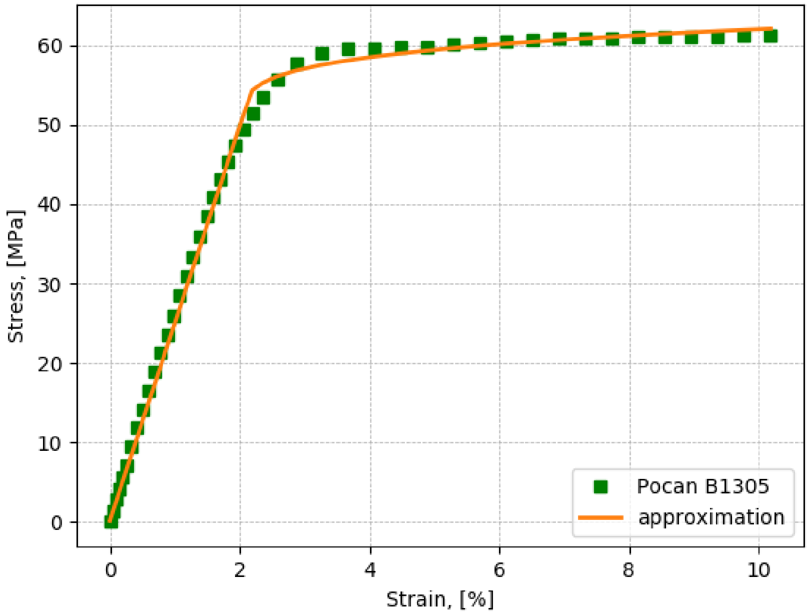

Figure 6.4: Approximation of the provided suppliers data for PBT

With approximation, the hardening modulus k and the hardening exponent m can be found. For the provided data the parameters are:

$$k = 22.78, \qquad m = 0.234504.$$

The procedure of obtaining the hardeing parameters is shown in Appendix A.1.

When the strain hardening parameters are determined, an appropriate model in Digimat can be defined. A comparison of the predicted response obtained by Digimat-MF with the suppliers data for Pocan B1305 is shown in Figure 6.5.

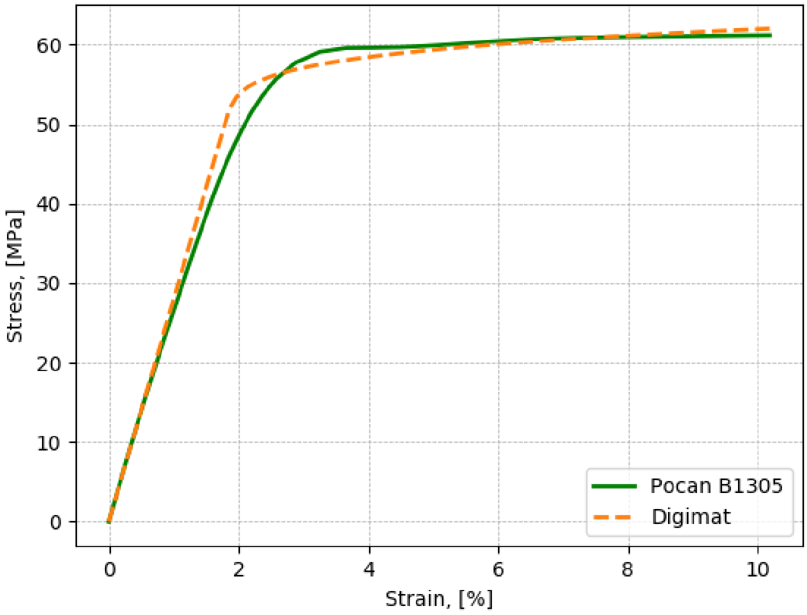

Figure 6.5: Comparison of predicted MF results with the suppliers data

6.3.2 2D vs. 3D RVE

An extensive analysis of PBT with various volume fractions of pores was carried out. A test case was simulated using a 2D and 3D RVE model for PBT with 2%, 4%, 6% and 8% of pores. All models have the same shape of pores with the average radius of pores of 50 μm. The properties of the matrix, PBT, are given in Table 2.1, with the hardening parameters $k = 22.78$ and $m = 0.234504$ as determined by the power law approximation.

A necessary step before the analysis of the mechanical behavior of PBT is to determine the number of inclusions at which the response remains unchanged. This is done by varying the size of the RVE for PBT with 2% pores on a 2D model and for PBT with 8% of pores on a 3D model. Only the RVE size was varied, and with that the number of pores present in the generated geometry, while the other parameters have been kept constant. In Digimat-FE, the first step is to generate the RVE. After that, an analysis is carried out using either the Digimat solver or the Abaqus solver. The 2D analysis is carried out with the built-in Digimat FE solver, while the 3D analysis is carried in Abaqus. The generated geometries for each respectable RVE alongside their respectable meshes are shown in Figure 6.6 for the 2D model and Figure 6.7 for the 3D model. Table 6.3 shows the number of elements for each mesh. For the 2D model, quadratic 6-node elements were used, while for the 3D model, quadratic tetrahedron elements C3D10M, which are described in Chapter 5, were used. The obtained responses are shown in Figure 6.8.

Table 6.3: The number of elements for each mesh of the 2D and 3D model used for RVE size variation

2D analysis		
PBT, 2% pores	RVE	Mesh
	0.5 mm, 3 inclusions	2131 elements
	1 mm, 10 inclusions	3140 elements
	1.5 mm, 23 inclusons	3696 elements
	2 mm, 41 inclusions	3342 elements
3D analysis		
PBT, 8% pores	RVE	Mesh
	0.15 mm, 4 inclusions	29859 elements
	0.2 mm, 10 inclusions	30293 elements
	0.25 mm, 19 inclusions	37753 elements
	0.3 mm, 33 inclusions	58189 elements

As seen in Figure 6.8, as long as the pore volume fraction remains the same, the homogenized response does not change significantly with the number of pores. For the 2D model, there is a slight deviation for 3 pores. It can be concluded that the size of the 2D RVE where the predicted response remains unchanged is 1 mm. For the 3D RVE, this size is 0.15 mm. It is recommended that the number of inclusions in a microstructure sample be at least 10 or more, but usually RVE's with around 30 inclusions are studied [22].

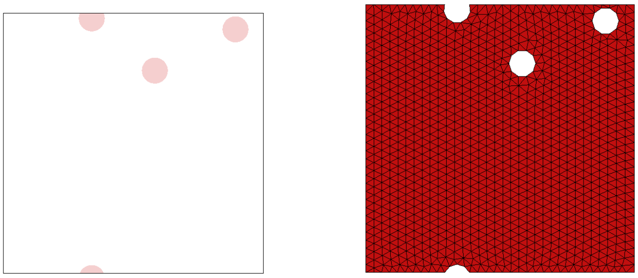

(a) RVE 0.5 mm **(b) RVE 0.5 mm, mesh**

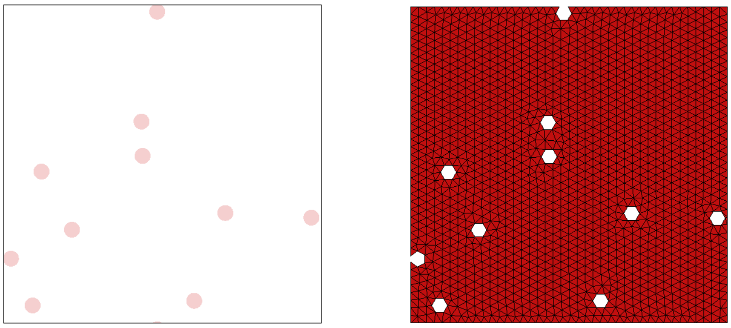

(c) RVE 1 mm **(d) RVE 1 mm, mesh**

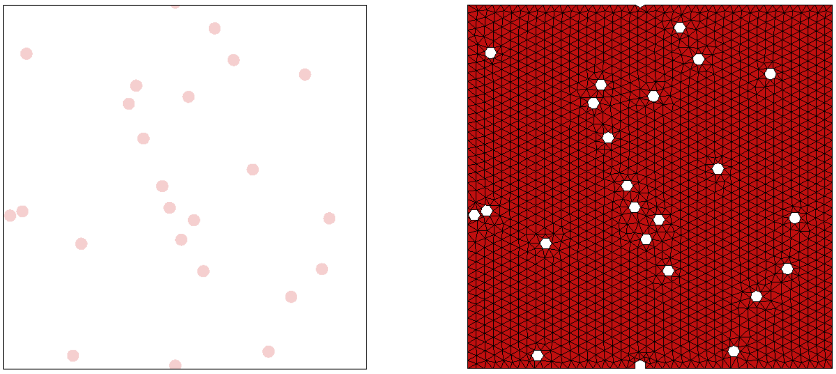

(e) RVE 1.5 mm **(f) RVE 1.5 mm, mesh**

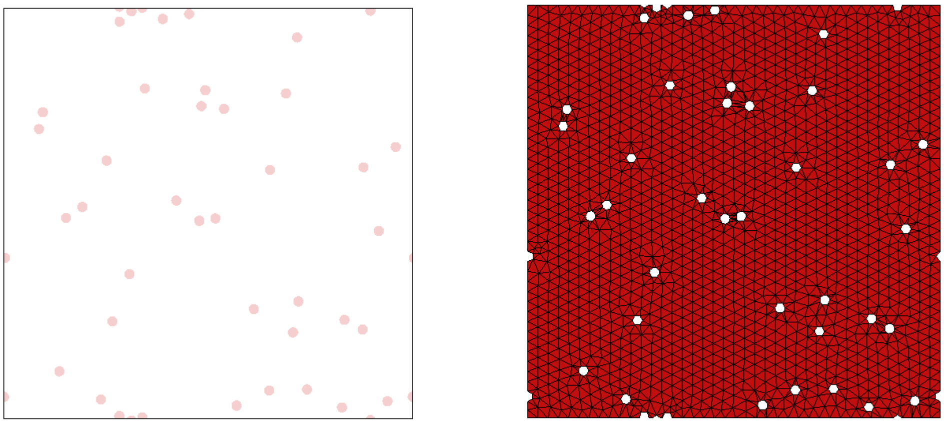

(g) RVE 2 mm **(h) RVE 2 mm, mesh**

Figure 6.6: RVE size variation: geometries and meshes of the 2D model for PBT, 2% pores

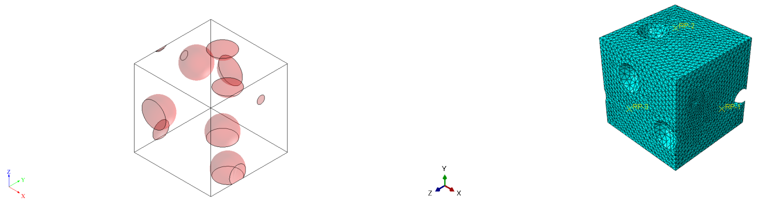

(a) RVE 0.15 mm **(b) RVE 0.15 mm, mesh**

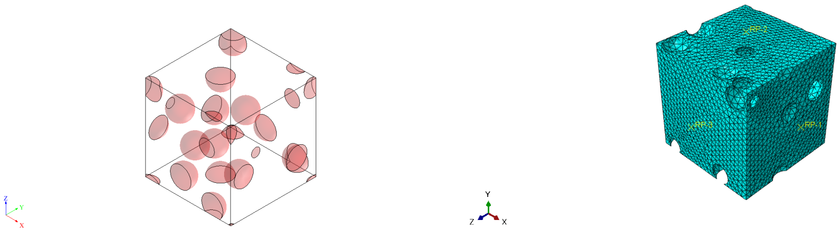

(c) RVE 0.2 mm **(d) RVE 0.2 mm, mesh**

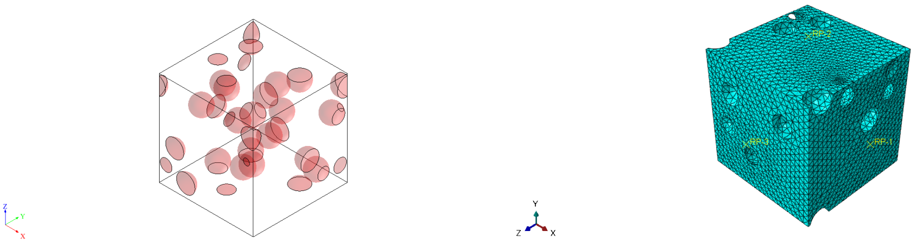

(e) RVE 0.25 mm **(f) RVE 0.25 mm, mesh**

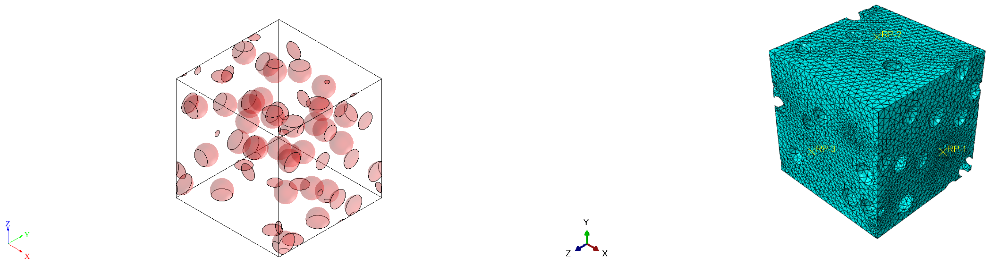

(g) RVE 0.3 mm **(h) RVE 0.3 mm, mesh**

Figure 6.7: RVE size variation: geometries and meshes of the 3D model for PBT, 8% pores

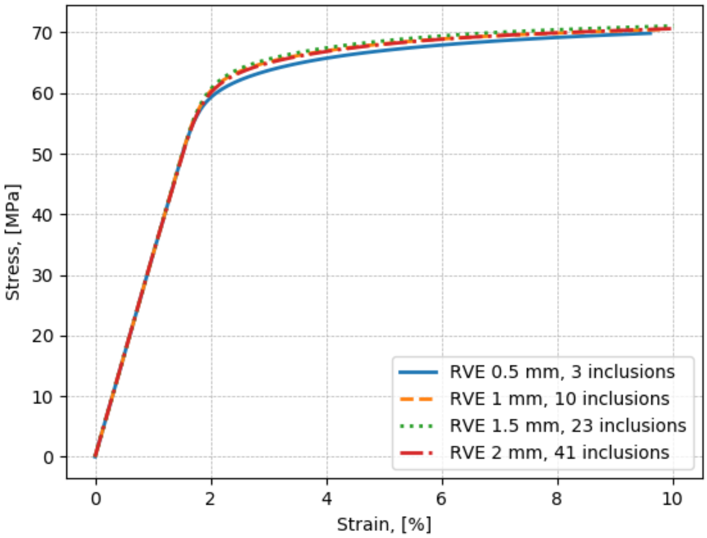

(a) 2D model, PBT, 2% pores

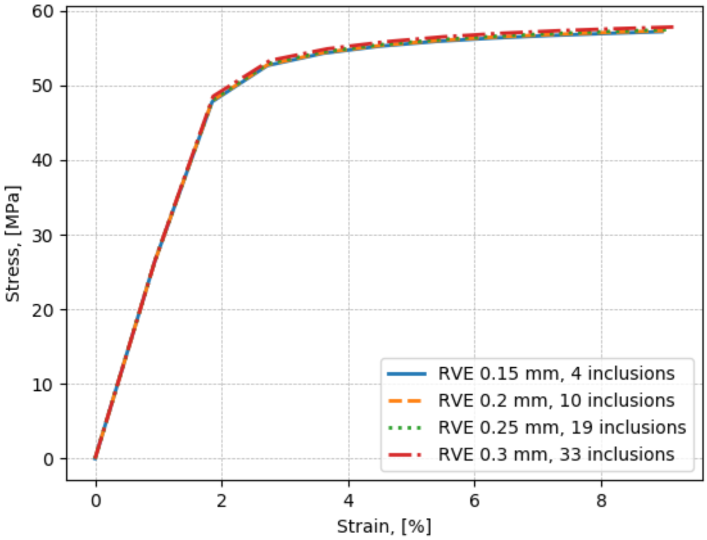

(b) 3D model, PBT, 8% pores

Figure 6.8: Comparison of the predicted responses for different sizes of the RVE

When generating the geometry of the RVE, randomness is included, therefore a test case was created to observe how the random geometry effects the predicted results. This test was carried out for PBT with 4% of pores on a 2D RVE model and for PBT with 8% of pores on a 3D RVE model. For both models, material properties of PBT were unchanged and the respective volume fraction of pores for each model was kept constant. Four test cases for both the 2D and 3D RVE model were created where the only changing parameter was the random distribution of pores. The generated geometries are shown in Figure 6.9 and Figure 6.10. The predicted responses are shown in Figure 6.11 and Figure 6.12. As both figures clearly show, the random geometry has no effect on the predicted response. This goes in hand with the assumption that geometry of the volume examined has no effect, hence the name of the representative volume element.

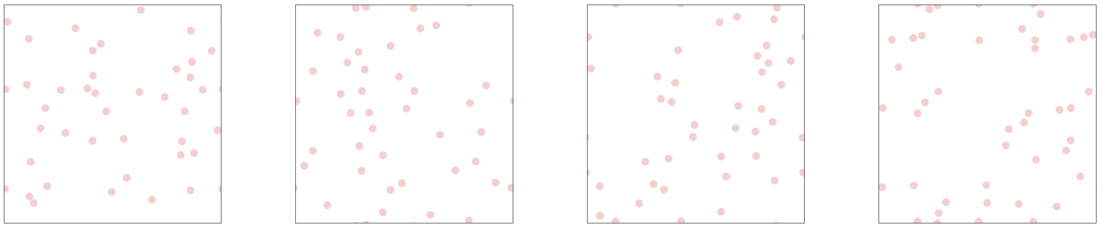

(a) Geometry 1 **(b) Geometry 2** **(c) Geometry 3** **(d) Geometry 4**

Figure 6.9: Random geometries for PBT with 4% of pores, 2D RVE

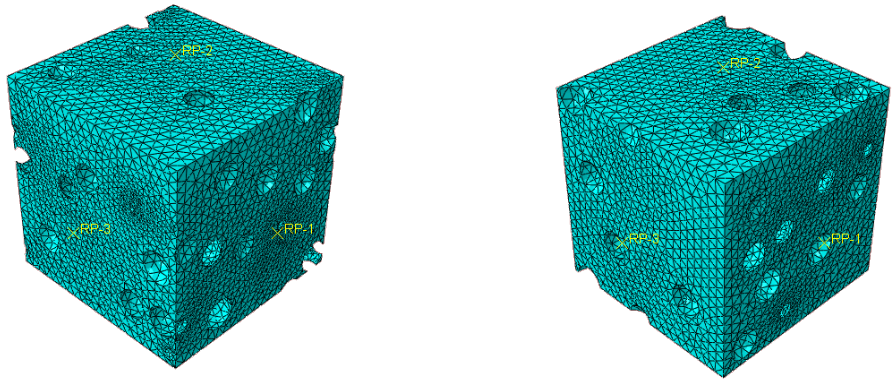

(a) Geometry 1 **(b) Geometry 2**

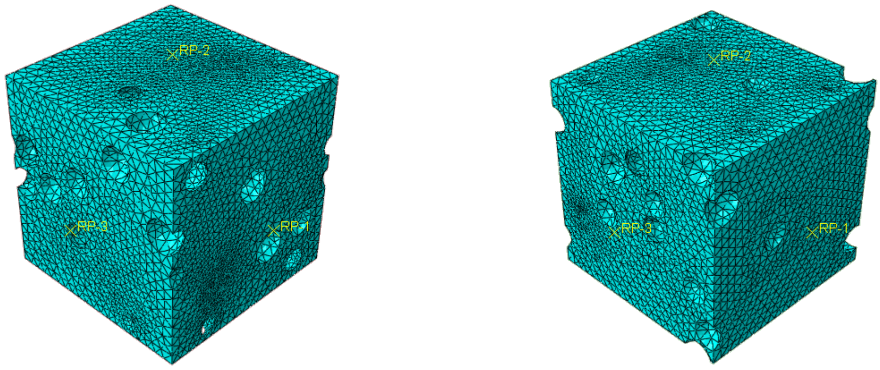

(c) Geometry 3 **(d) Geometry 4**

Figure 6.10: Random geometries for PBT with 8% of pores, 3D RVE

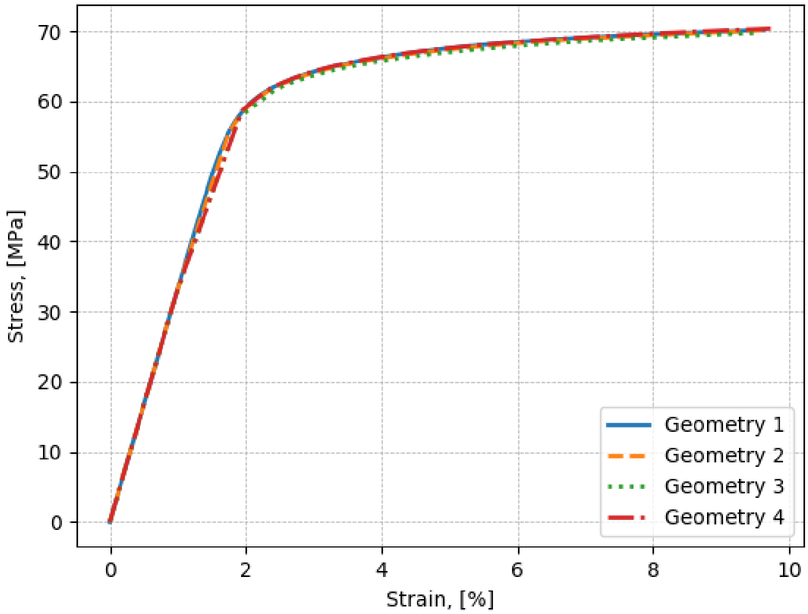

Figure 6.11: Predicted responses for PBT with 4 % of pores for different cases of random geometry (2D RVE)

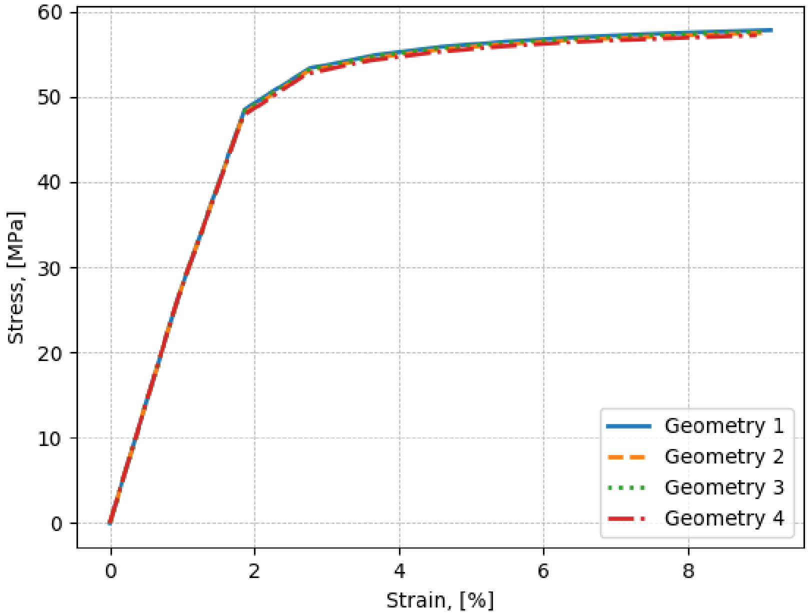

Figure 6.12: Predicted responses for PBT with 8 % of pores for different cases of random geometry (3D RVE)

Furthermore, the effect of pore size is tested on a 3D RVE model for PBT with 2 % of pores. The size of pores is increased and responses for the following values are obtained: 50 μm 100 μm, 200 μm and 500 μm.

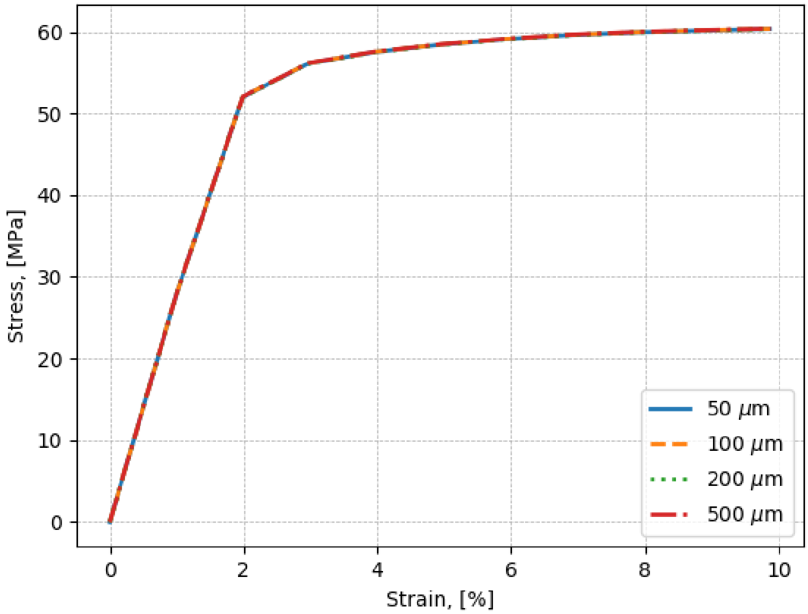

Figure 6.13: The effect of pore size on the predicted response for PBT, 2% pores

As Figure 6.13 shows, pore size has no effect on the average results, for spherical pores.

The next step is the variation of the pore volume fraction on a 2D RVE model. For every volume fraction of pores a different RVE was used. For 2% of pores, the size of RVE is 2 mm; for 4% of pores 1.4 mm, for 6% and for 8% of pores the RVE size is equal and its value is 1 mm. The results of the 2D case show an unexpected response (Figure 6.14). The predicted values with the 2D RVE are higher than expected, the reason being that 2D RVE's give accurate predictions only for microstructures which are consisting of a matrix and long unidirectional fibers [17]. Given that the created a 2D model has a geometry with pores which are small in size and have low aspect ratios, the predictions are inaccurate.

The results obtained on the 3D RVE differ from the 2D case and give a much better prediction (Figure 6.15).

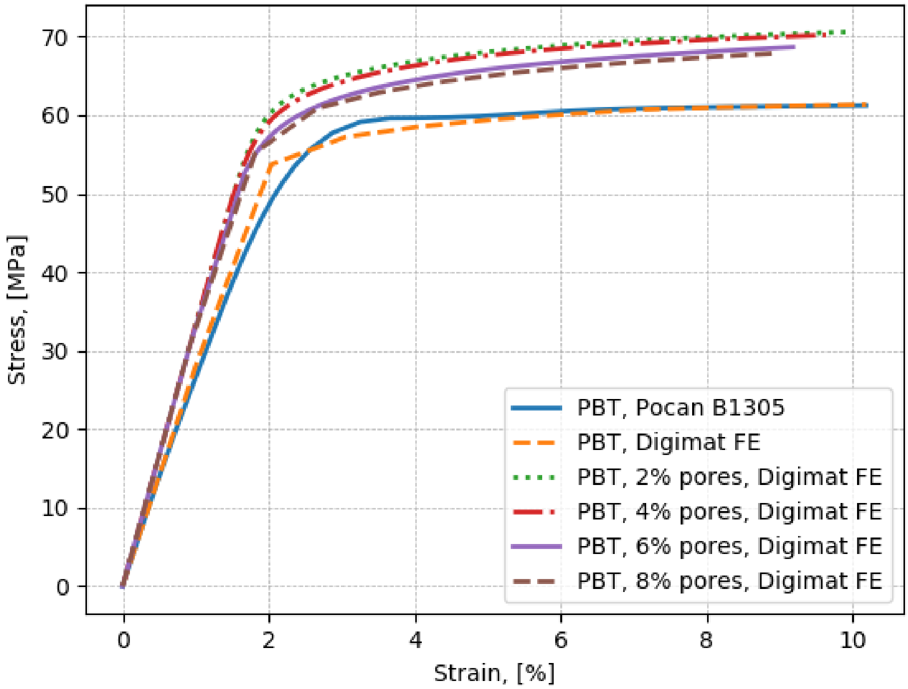

Figure 6.14: **Comparison of predicted responses with 2D analysis for PBT with different volume fractions of pores**

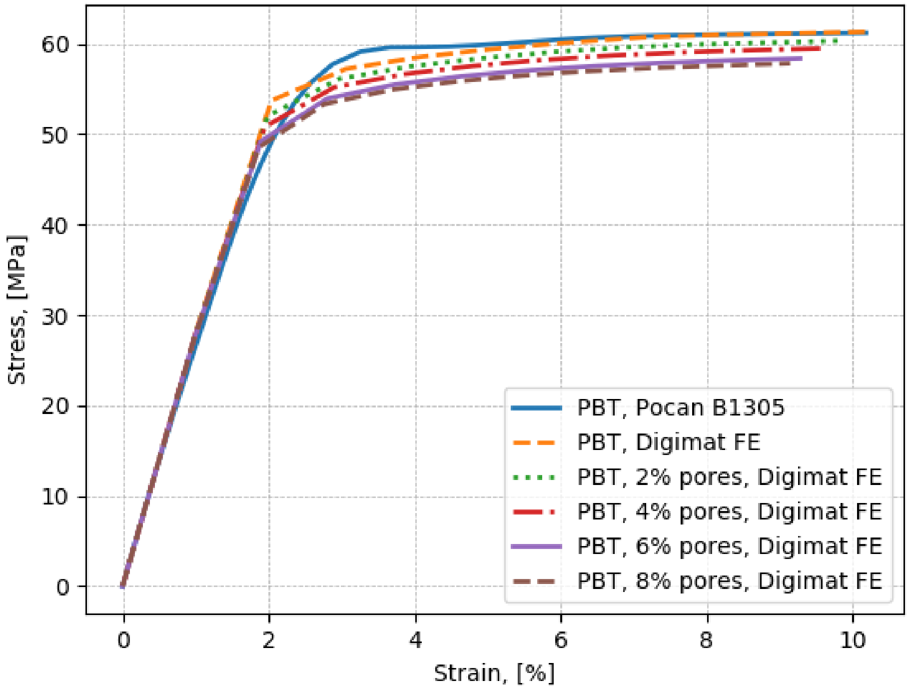

Figure 6.15: **Comparison of predicted responses with 3D analysis for PBT with different volume fractions of pores**

Figure 6.16 shows a comparison of the predicted responses with 2D and 3D analysis. Although it was expected for the results to be nearly matched, this is not the case. The 2D model, although less computationally expensive, gives wrong predictions for the reasons mentioned earlier. Therefore, 3D RVE models were used for all subsequent analyses.

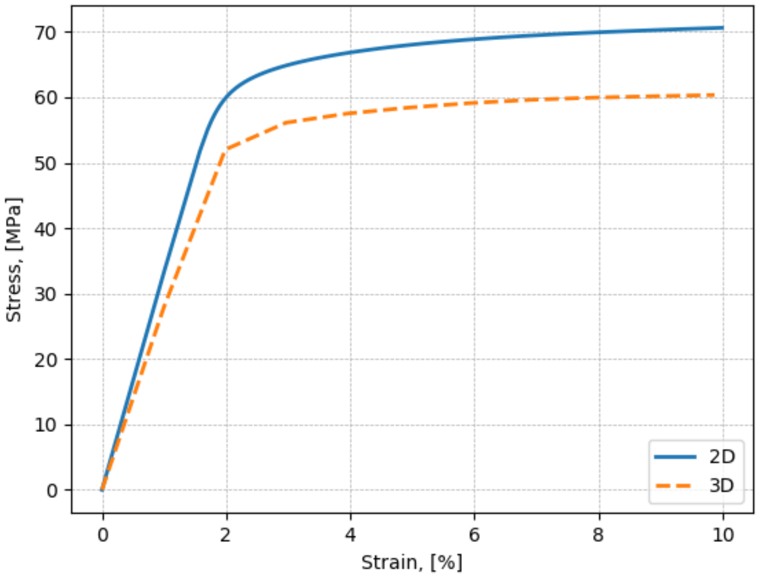

(a) PBT, 2% pores

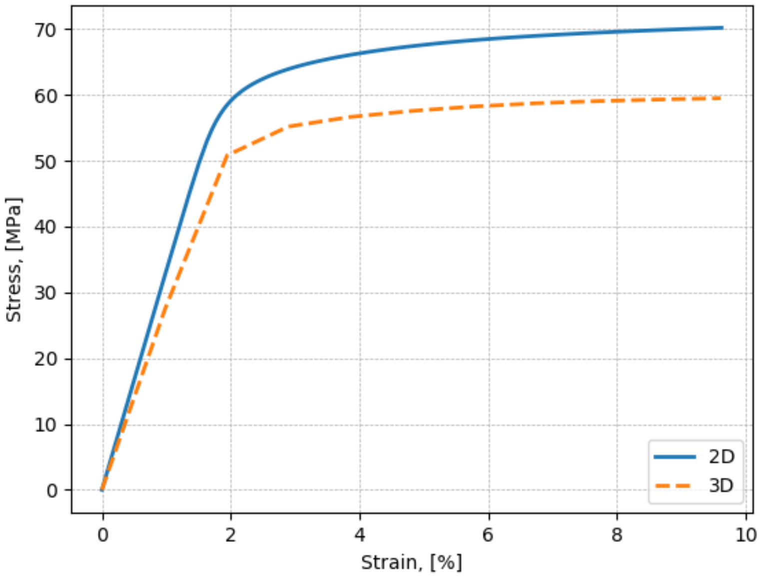

(b) PBT, 4% pores

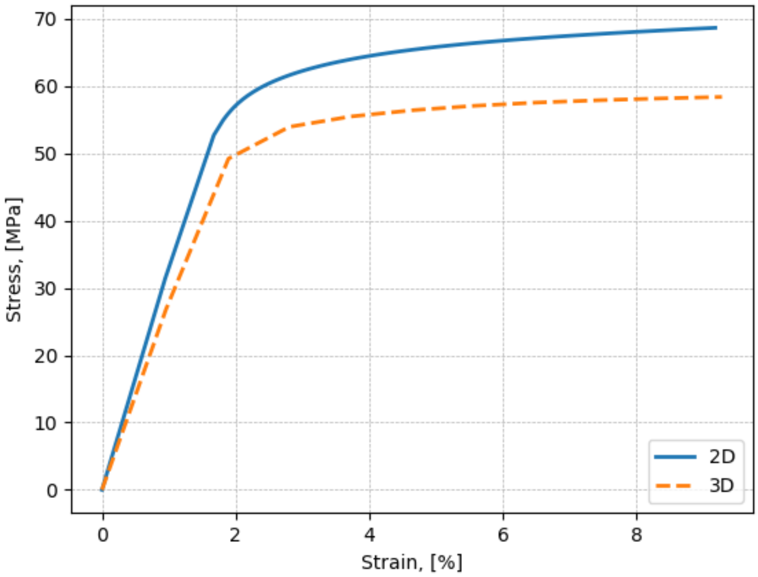

(c) PBT, 6% pores

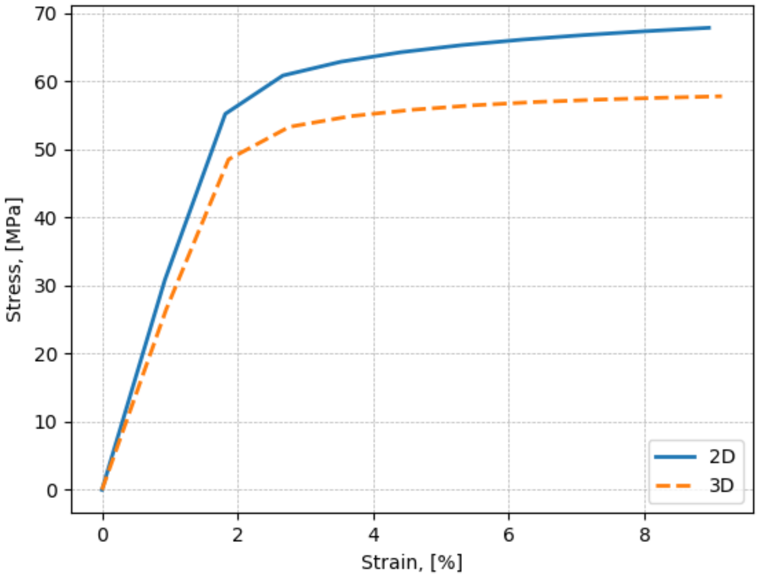

(d) PBT, 8% pores

Figure 6.16: Comparison of the predicted responses obtained with 2D and 3D analysis for PBT: a) 2%, b) 4%, c) 6%, d) 8% of pores

6.3.3 Mori-Tanaka Method

For a reference, a prediction was acquired with Digimat MF by using the Mori-Tanaka homogenization model. The comparison is visible in Figure 6.17.

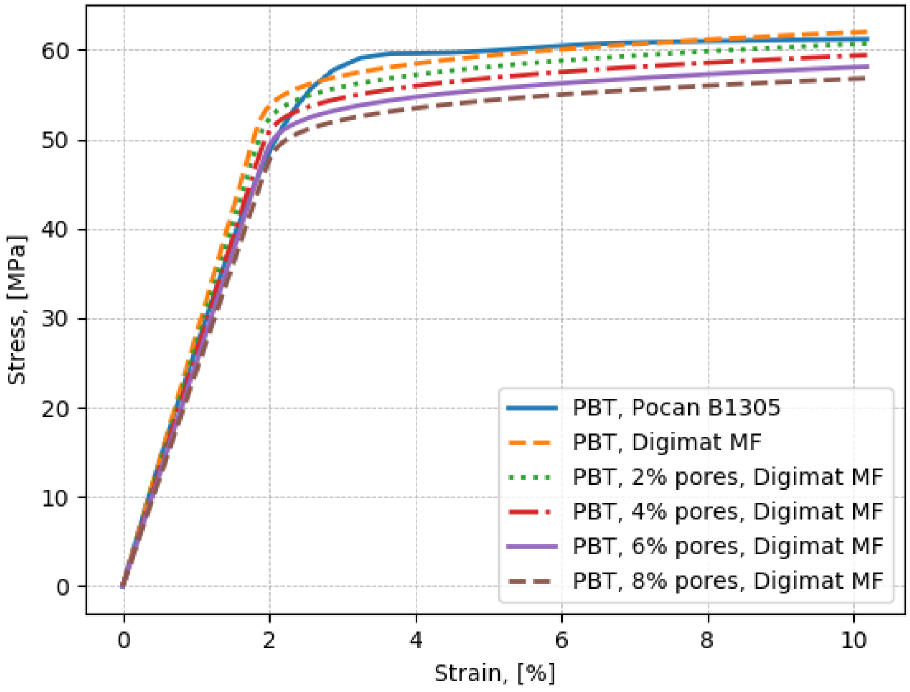

Figure 6.17: The effect of pores on the response of PBT

Figure 6.18 shows the comparison of the predicted responses with Digimat MF and the 3D RVE model in Digimat FE. It clearly shows a good match of results, with a note that Digimat MF doesn't predict the maximum strain values correctly when pores are present, compared to the analysis carried out on a RVE, which is clearly seen in the figures below. The reason for this discrepancy is that the Mori-Tanaka method does not take the geometry into account when homogenization is carried out. The maximum strain value drops from 10.181 % for pure PBT to 9.142 % for the microstructure with 8% of pores in the case of a 3D RVE. The Mori-Tanaka approach can still give a good indication when there are time constraints, because the computation time for that approach is several times lower.

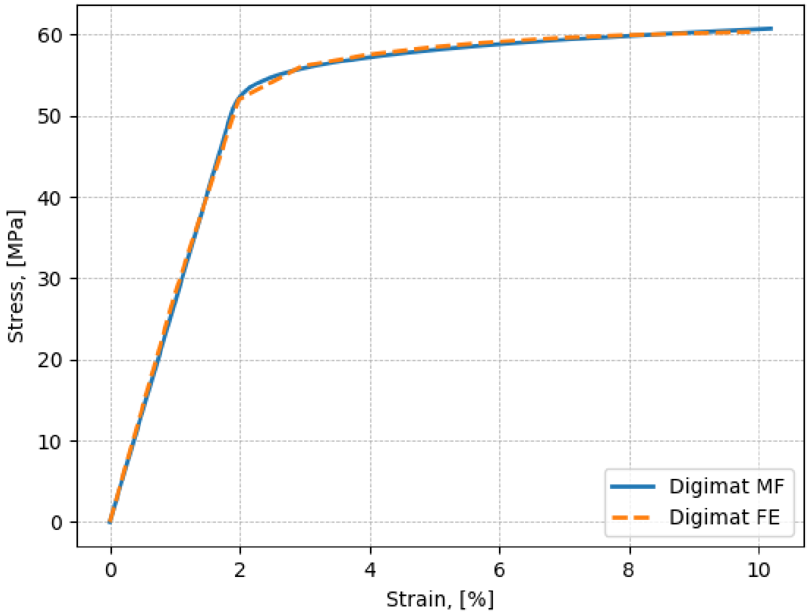

(a) PBT, 2% pores

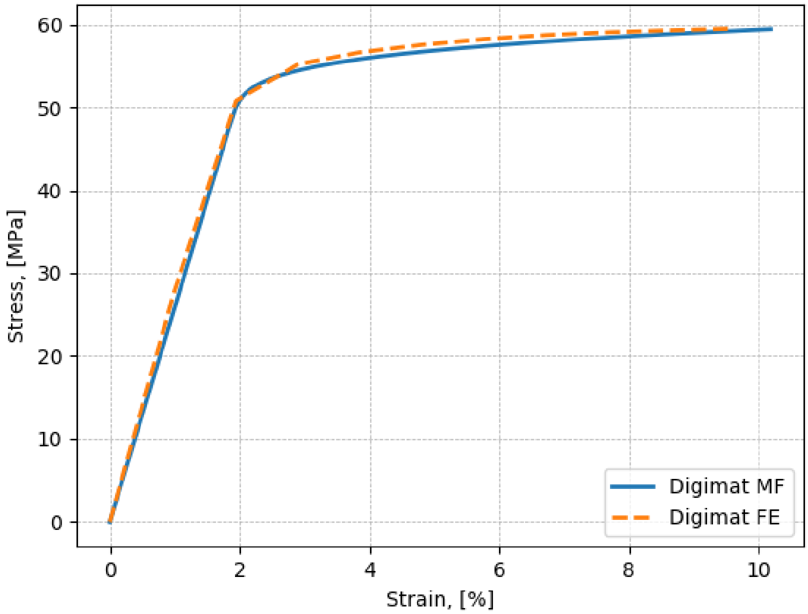

(b) PBT, 4% pores

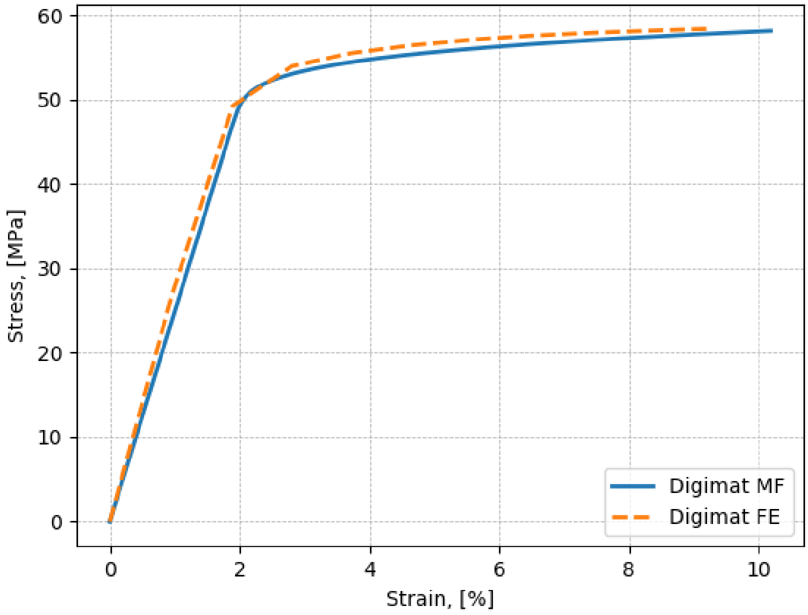

(c) PBT, 6% pores

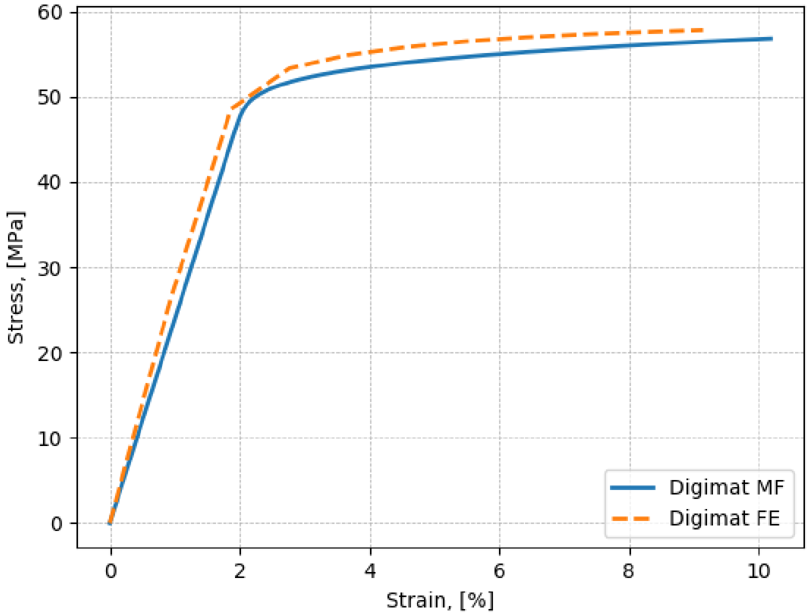

(d) PBT, 8% pores

Figure 6.18: Comparison of the predicted responses obtained with Digimat MF and Digimat FE

6.3.4 3D RVE - large strain theory

Next, the results obtained with the assumption of large strains are shown. Figure 6.19 shows the comparison of predictions with small strains and large strains (NLGEOM). The geometric non-linearity is taken into account by toggling the NLGEOM option in Abaqus.

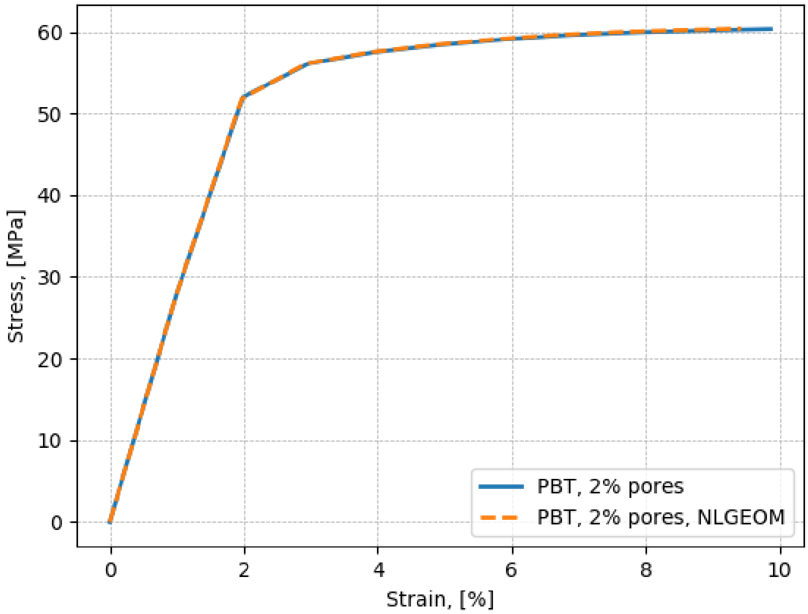

(a) PBT, 2% pores

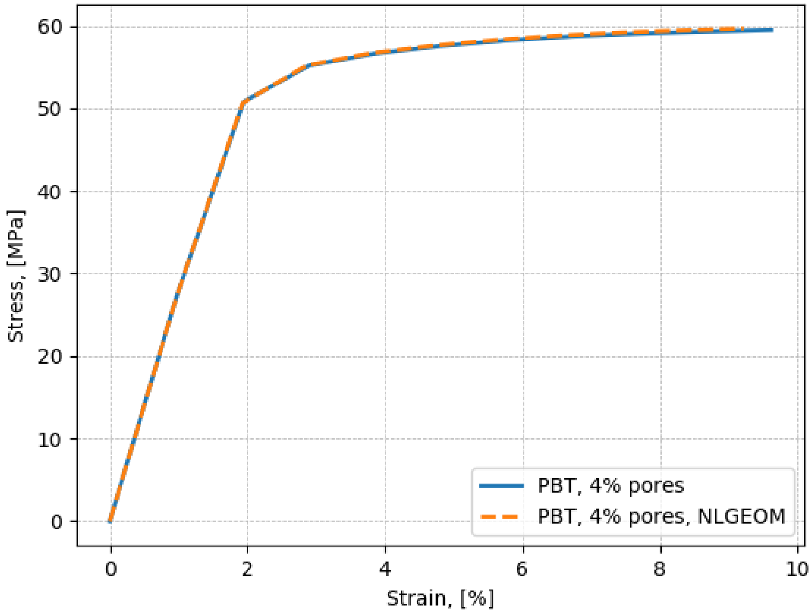

(b) PBT, 4% pores

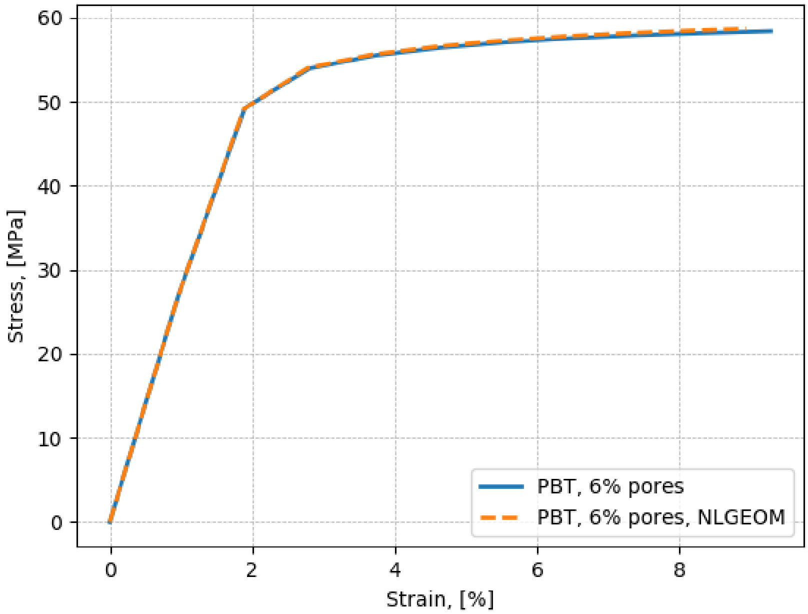

(c) PBT, 6% pores

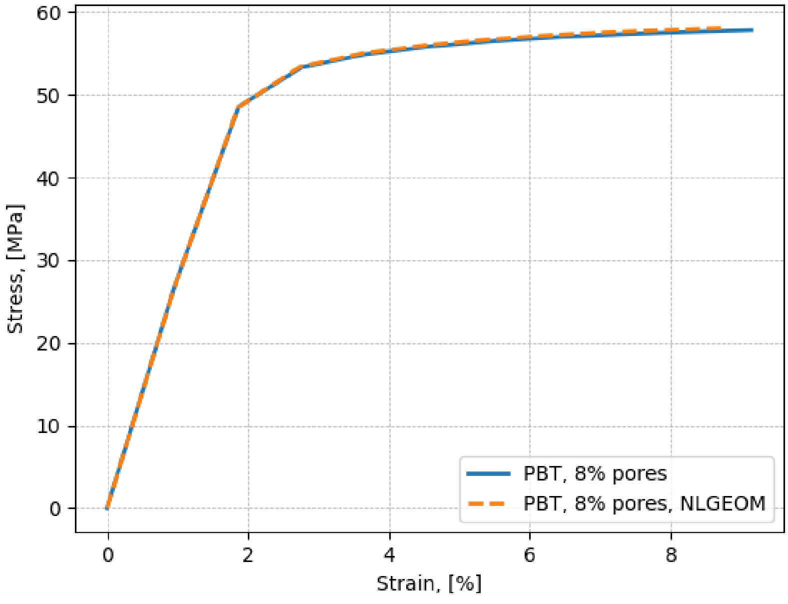

(d) PBT, 8% pores

Figure 6.19: Comparison of predicted responses with small strain theory and large strain theory (NLGEOM): a) 2%, b) 4%, c) 6%, d) 8% of pores

It can be clearly seen that the large strain theory predicts smaller strains, i.e. the model is stiffer. The difference, although, is negligible because PBT exhibits elastic-ideal plastic behavior and the model can be simplified by using the small strain theory.

Next, a comparison of the responses predicted with large strain theory with the suppliers data for PBT can be seen in Figure 6.20.

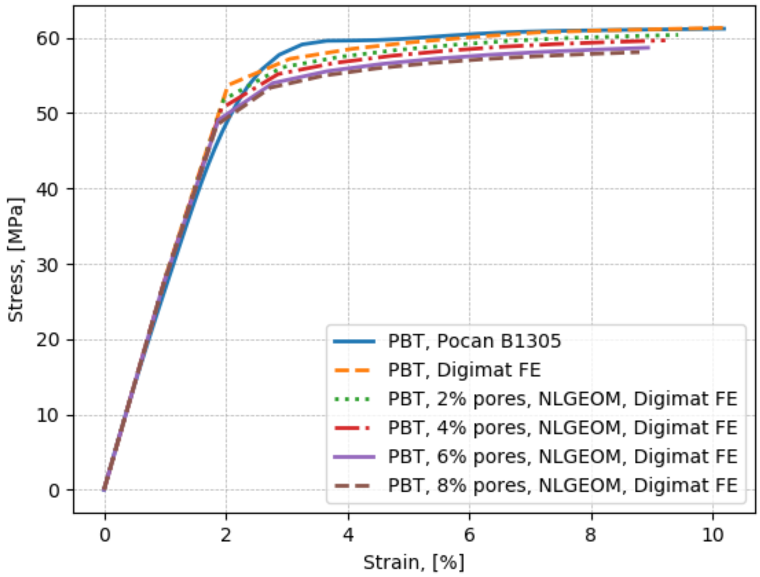

Figure 6.20: Comparison of predictions with 3D RVEs and assumption of large strains for PBT with different pore volume fractions

Finally, Figure 6.21 shows the correlation of the volume fraction of pores versus the total strain as predicted by small strain and large strain theory. As the volume fraction of pores rises, the maximum strain values become smaller. At 8% of pores, for small strain theory the strain value is 9.14% and for large strain theory 8.79%.

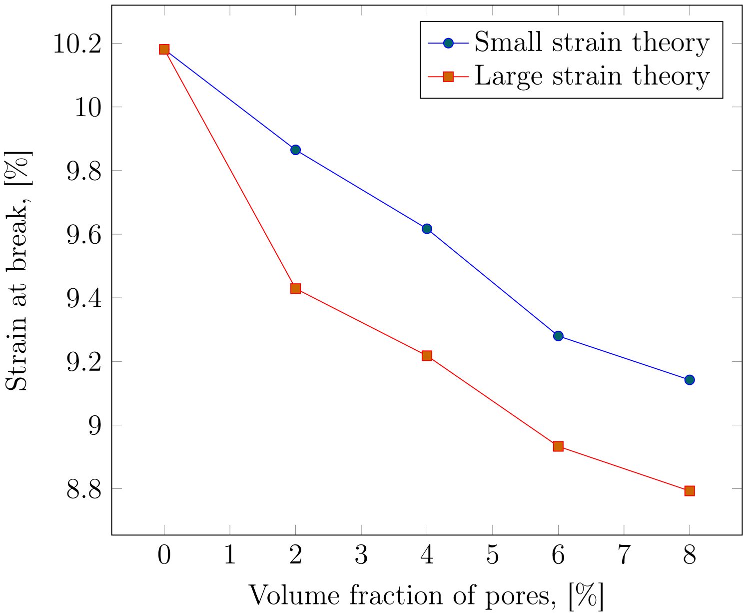

Figure 6.21: Volume fraction vs. strain - 3D RVE

6.4 Tension test verification

A tension test implies an uniaxial or biaxial test where a controlled tension is applied to a specimen until failure occurs. A tension test makes it possible to measure the reduction in area section, ultimate tensile strength, maximum elongation and breaking strength. From these measurements Young's modulus, Poisson's ratio, yield strength, and strain-hardening constants can be determined.

The goal is to show how various percentages of pores included in the material affect the strength of the material. Therefore, a simple tension specimen has been created and subjected to tensile loads, for the purpose of showing that for the same geometry, loads and boundary conditions the material imperfections have an effect on the strength of the material.

The analysis was carried out in two FE software packages, namely: Abaqus and Digimat. Digimat is a software for modeling microstructures and mapping the micro level to the macro level. A comparison of results obtained with this coupled analysis was compared to the predictions with the 3D RVE.

The tension test was carried out on a standard tensile test specimen. The dimensions of the specimen under examination are: 10 x 4 x 80 mm (width x thickness x length). The cross-section is shown in Figure 6.22.

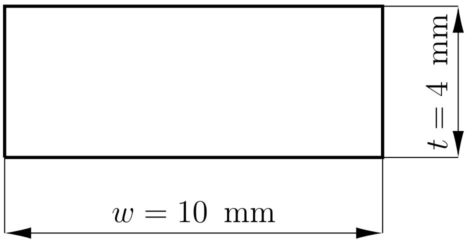

Figure 6.22: Cross-section area of the tension specimen

The load, boundary conditions and mesh can be seen in Figure 6.23. The lower part is fixed, and the upper part is supported, allowing displacement in the global direction Y. On the upper end of the specimen a displacement is prescribed that corresponds to the maximum strain of 10.18%, also in the direction of Y. Therefore, a displacement of $u = 8.145$ mm is prescribed. The geometry is discretized with 190 quadratic elements of type C3D20R.

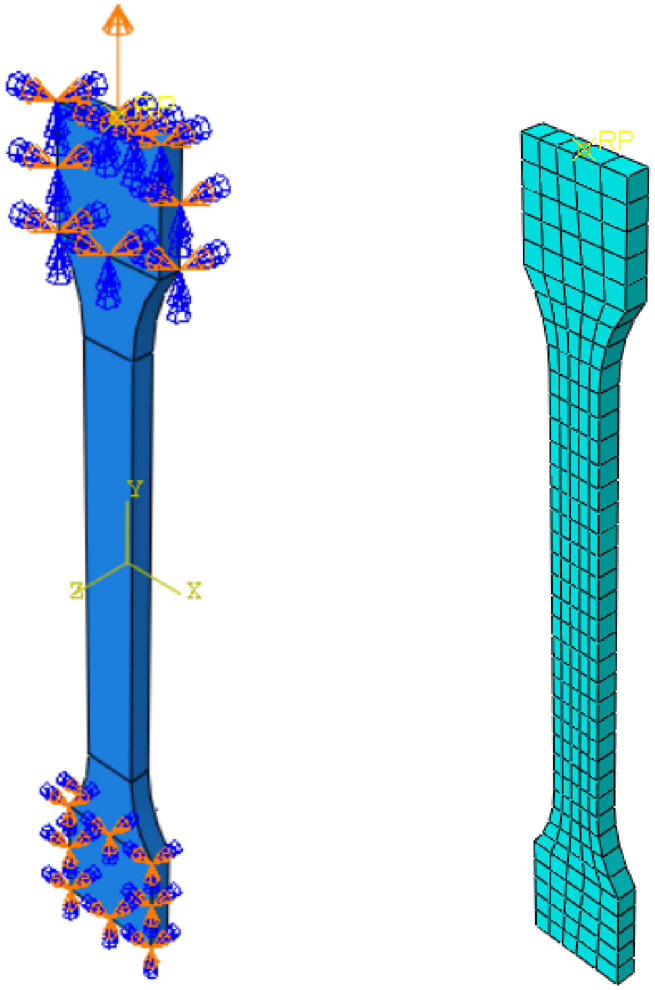

(a) Load and BC's **(b) Mesh**

Figure 6.23: Load, boundary conditions and mesh of the tension specimen

The coupled analysis in Digimat CAE and Abaqus is created through a modified input file where all the parameters are defined according to the usual input file structure, with the difference that the material is updated from the microstructure defined in Digimat CAE. The input file can be seen in Appendix A.2. One advantage of this approach is that homogenization can be applied to real geometry. Furthermore, the computation time is greatly reduced if the geometry is simple and mesh density isn't too high. The predicted responses are comparable to the 3D RVE analysis, with a noticeable discrepancy as the volume fraction of pores increases.

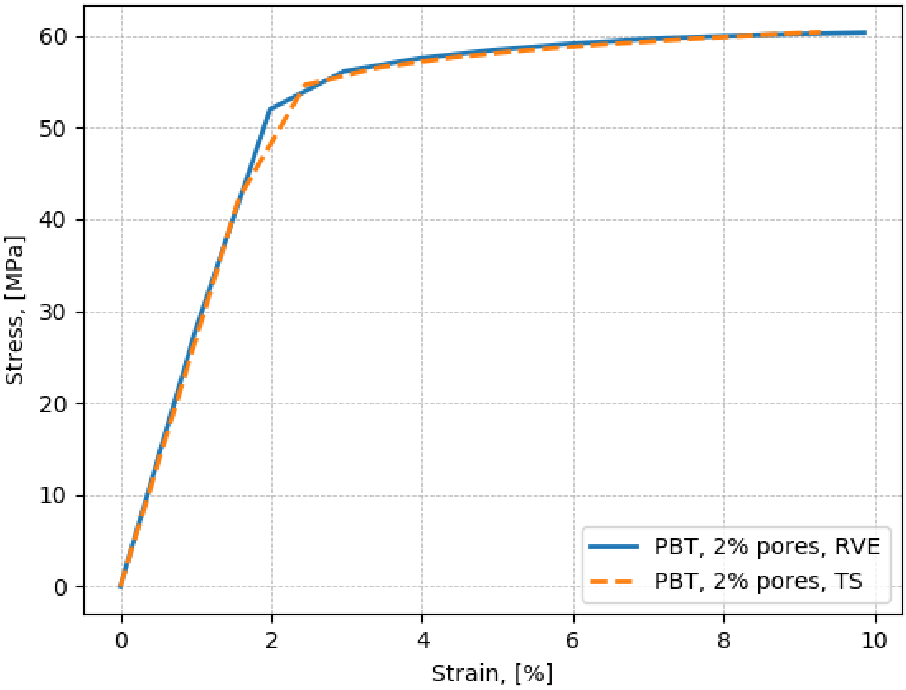

(a) PBT, 2% pores

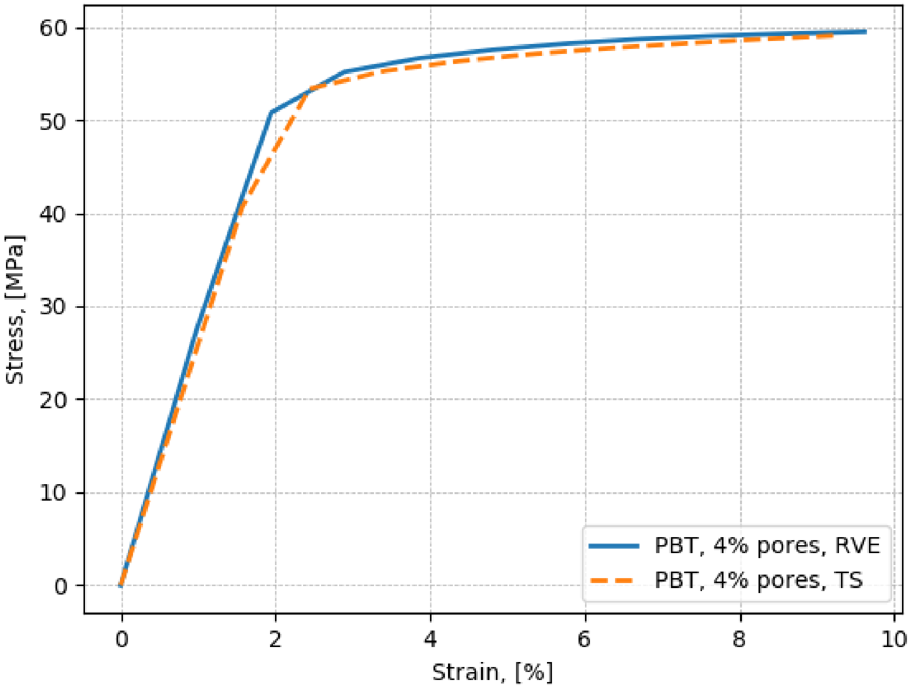

(b) PBT, 4% pores

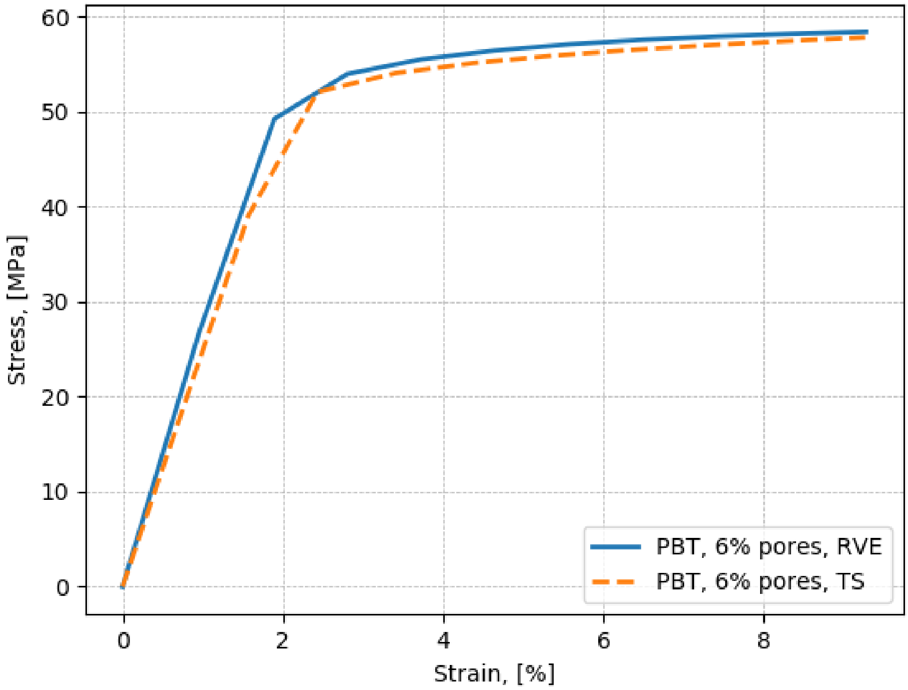

(c) PBT, 6% pores

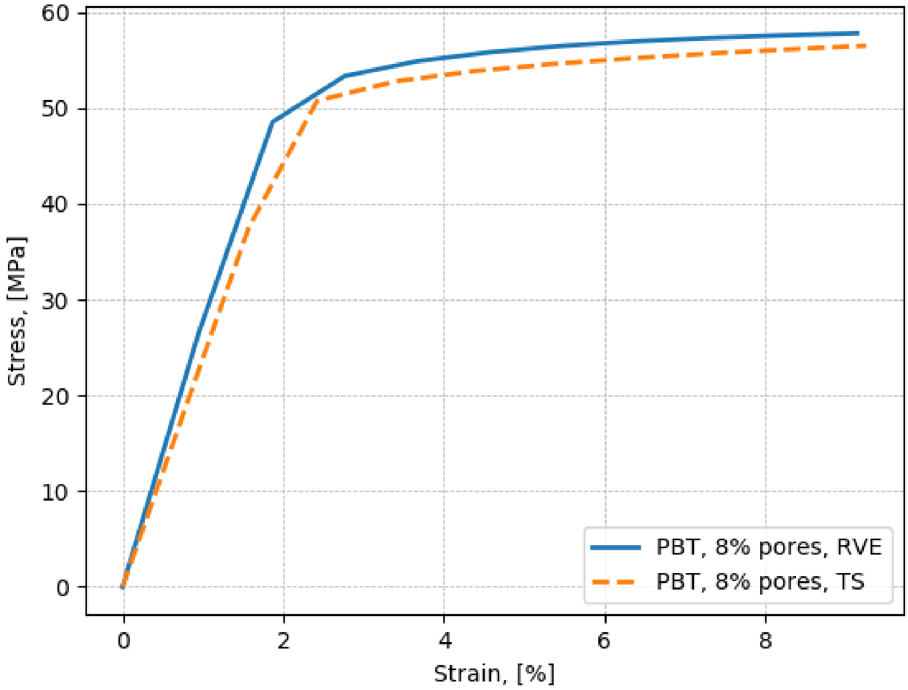

(d) PBT, 8% pores

Figure 6.24: Comparison of the predicted responses obtained with a 3D RVE and a coupled Digimat-Abaqus analysis of a tension specimen

6.5 Experimental results

The experiment was carried out in cooperation with Yazaki Europe Ltd. - Zagreb branch. Tension specimens of pure PBT resin and porous PBT were tested. To induce the occurrence of air bubbles, PBT was mixed with 1% of Hydrocerol chemical foaming. After the expansion of the chemical foaming, air bubbles ensue in the specimens where Hydrocerol was added. To obtain the necessary data to define the pore phase, tomography is used. This procedure is carried out on a CT machine to obtain section images of an object. More about the concepts of tomography and its use in mapping of porous materials can be learned in [39].

Porous tension specimens are scanned and information about their microstructure can then be obtained with the use of a dedicated software accompanying the CT machine. Two porous specimens are scanned and the information about their pore phase can be seen in Table 6.4.

Table 6.4: Experimental data for the pore phase

Specimen	Pore radius [mm]	Volume fracion of pores [%]
PBT B1305, 1% Hydrocerol, Specimen #1	0.081	0.95
PBT B1305, 1% Hydrocerol, Specimen #3	0.1225	2.01

Furthermore, a tension test is carried out for pure PBT B1305 to obtain the necessary data of the matrix phase. After that, two 3D RVE models are created, each representing the microstructure of the appropriate specimen according to Table 6.4. The 3D RVE models are shown in Figure 6.25

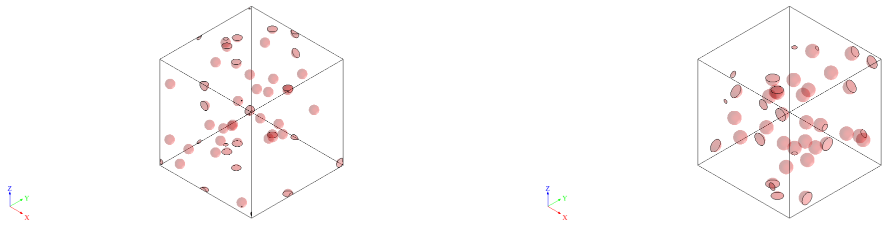

(a) Specimen #1

(b) Specimen #3

Figure 6.25: Microstructure of PBT B1305, 1% Hydrocerol: a) Specimen #1, b) Specimen #3

The necessary parameters of the matrix phase (PBT 1305) are obtained from the experimental stress strain-curve of pure PBT B1305 by the procedure shown in Subsection 6.3.1. The parameters for defining the elasto-plastic model of pure PBT B1305 are shown in Table 6.5.

Table 6.5: Parameters for defining the elasto-plastic material model, PBT B1305

E [MPa]	ν [-]	k [-]	m [-]
2400	0.3981	2.54	0.169531

The experimental stress-strain curve of PBT 1305 and the approximation of said curve are shown in Figure 6.26.

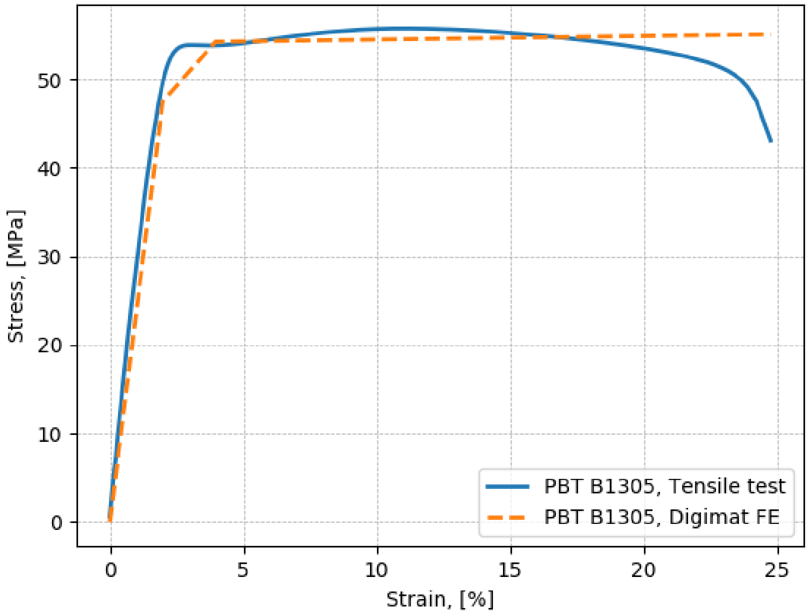

Figure 6.26: Experimental stress-strain curve of PBT 1305 and its approximation in Digimat FE

Finally, the predicted responses of a 3D RVE model obtained with Digimat FE are compared to the experimentally obtained stress-strain curves for PBT 1305 with 1% Hydrocerol. Figure 6.27 shows the comparison of the predicted responses with experimental data for Specimen #1 and Specimen #3. In the linear elastic regime, there is good match of results for both specimens. In the plastic regime, there is a considerable discrepancy between experimental data and the prediction obtained with the use of a representative volume element. The prediction overestimates the response compared to experimental results. It is known that homogenization doesn't always yield accurate results in the plastic regime [21], therefore a better procedure for that regime has to be found. For a further elaboration see the section 6.6 Discussion.

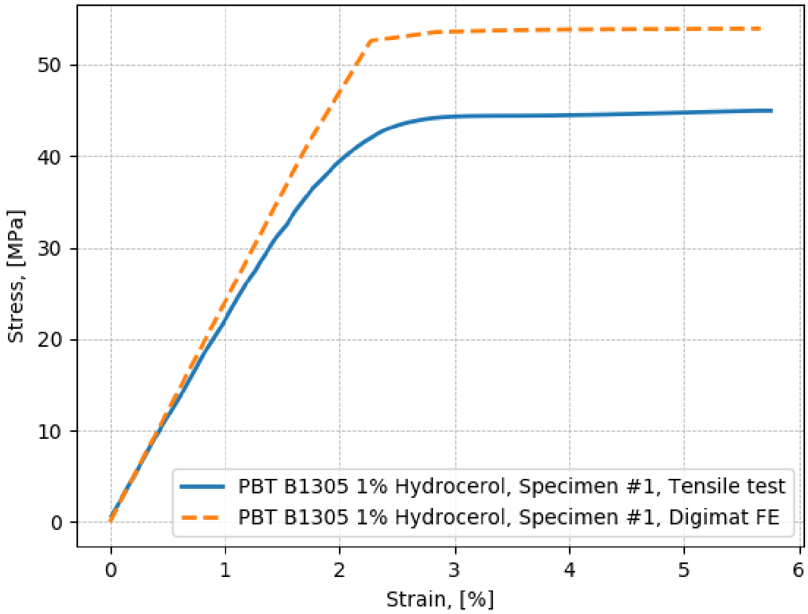

(a) **Specimen #1**

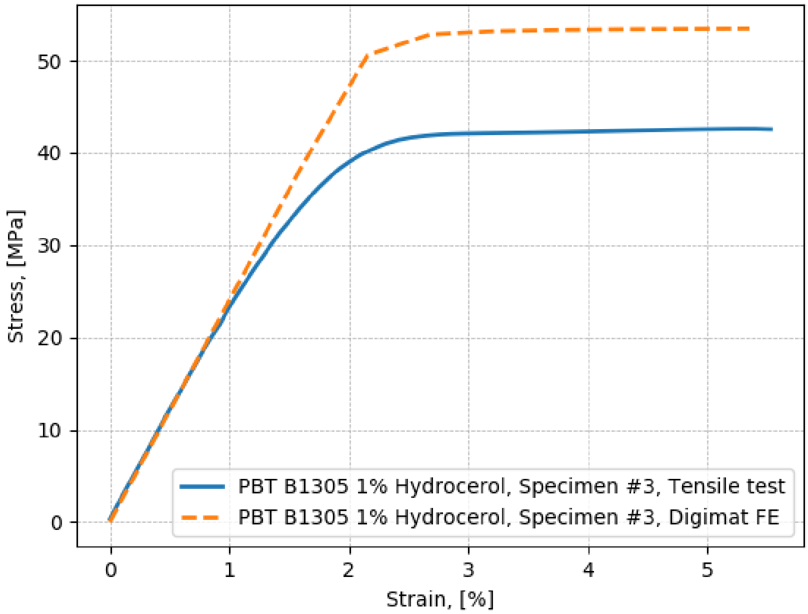

(b) **Specimen #3**

Figure 6.27: Comparison of experimentally obtained data with predicted responses obtained with Digimat FE for PBT 1305, 1% Hydrocerol: a) Specimen #1, b) Specimen #3

6.6 Discussion

An elasto-plastic model for PBT is used for the prediction of its mechanical behavior. After the definition of the material model, verification of used methods is carried out. Then, the results of a tension test simulation are compared with the results obtained through a simulation of a RVE. Finally, the results obtained by the simulation of a 3D RVE are compared to experimental data for PBT B1305.

By increasing the size of the RVE, it is shown that a minimal size, where the microstructure sample is representative of the material behavior, can be determined. If the size of the RVE is increased beyond that limit, no change in the predicted response is observed. The change of distribution of pores and the size of pores also has no effect on the predictions. Furthermore, it is shown that a 3D RVE yields better predictions than a 2D RVE and the Mori-Tanaka method. The approach where large strains are employed does not show a considerable difference in predicted responses when compared to the results obtained with small strain theory. A coupled Digimat-Abaqus simulation of a tension specimen yields less accurate results, but greatly reduces the computation time.

The analysis of mechanical behavior of PBT resin has shown that the predictions obtained with homogenization, when compared to experimental results, are accurate in the linear elastic regime. In the plastic regime, the predicted response drifts away from experimental data by overestimating the actual response.

The reasons for this overestimation lies in the fact that homogenization does not always yield accurate predictions in the plastic regime. Furthermore, it was assumed that the shape of pores is spherical, to avoid numerical problems with rough edges. This way, the possibility that stress concentration will invalidate the results is reduced. With the assumption that all pores are identical in terms of shape and size and modeled as spheres also contributes to the error. Another possibility for the discrepancy is that the properties of PBT 1305 are deteriorated with the addition of Hydrocerol during the injection molding process, and this behavior cannot be captured with this approach. With all of the above in mind, steps that tackle those issues must be taken to solve this problem.

7 Conclusion

The thesis deals with the impact of porosity on the mechanical properties of PBT. For various percentages of pores in the PBT resin, it was shown that the strength of PBT decreases. This results in breaking of components made of such defective materials earlier than expected. The objective of this study is to predict the behavior of PBT with pores present. A multi-scale approach is taken, where the microstructure of PBT is observed and its effect on the macro results is taken into account.

First, a research of PBT and its properties is carried out. This material exhibits outstanding mechanical, thermal and electrical properties and because of that it is used in a wide range of applications. If reinforced with fibers, even better mechanical properties can be obtained. Usually, glass fibers are used as a reinforcing component. The most common variants are PBT with 20% of glass fibers (PBT-GF20) and PBT with 30% of glass fibers (PBT-GF30). It exhibits great ductility, which is why an approximation by Ramberg-Osgood approach was considered, but, unfortunately, none of the variants (PBT, PBT-GF20, PBT-GF30) obey the Ramberg-Osgood law.

In this thesis, PBT is modeled as an elasto-plastic material where the von Mises yield criterion is used. The isotropic hardening is modeled with a power law. The approximation of the isotropic hardening with the power law yields the isotropic hardening parameters which are used to define a constitutive material model in a FE analysis. This approach makes it possible to predict the effect of porosity in the plastic regime.

The analysis of the constitutive mechanical behavior of PBT, where porosity is included, is determined by means of homogenization methods. The concept of a representative volume element (RVE) is introduced. The RVE is a sample of the microstructure of the material. Periodic boundary conditions, which link the micro and macro scale are applied to the RVEs boundary. The displacements at the RVE boundaries are prescribed to correspond to the macro strain. An FE analysis of the microstructure is then carried out and volume average stress and strain fields are obtained. With this approach, material properties of PBT can be obtained by simulating only a small part of the material, thus achieving a great reduction in computation time. An approach with the Mori-Tanaka method is also taken, where the anisotropy of porous PBT is described with the known characteristics of constituents (PBT, pores). This approach simplifies the modeling phase, but it is only accurate for volume fractions of inclusion phase which are lower than 25%.

The analysis of the mechanical behavior of porous PBT was carried out in Digimat and Abaqus. The process consisted of generating the microstructure in Digimat and carrying the FE analysis either in Digimat or Abaqus. Firstly, the size of the RVE at which the microstructure sample is representative was determined. For a 2D RVE, the size was 1 mm with 10 inclusions, and for a 3D RVE the size was 0.15 mm with 4 inclusions. It has been demonstrated that distribution of pores doesn't affect the volume average stress and strain fields if spherical pores are modeled. Furthermore, the size of pores also didn't influence the predicted response, if the volume fraction of pores remained constant. With increase of the volume fraction of pores, the strength of PBT was lower compared to pure PBT. It was determined that the 2D RVE overestimates the mechanical response of PBT, while the 3D RVE yields better predictions. It was also shown that the effect of geometric nonlinearity is negligible.

Finally, the predicted mechanical response of PBT 1305, obtained through the employment of a RVE, was compared to an experimentally obtained result. The comparison showed that the prediction is accurate in the linear elastic regime, but, in the plastic regime, this was not the case. Therefore, a further investigation of homogenization in the plastic regime, as well as experimental measurements, is recommended.

References

[1] V. Kobelev: Design and Analysis of Composite Structures for Automotive Applications, Wiley-VCH, 2019; DOI: `https://doi.org/10.1002/9781119513889`; Available online at: `https://www.researchgate.net/publication/330702957_Design_and_Analysis_of_Composite_Structures_for_Automotive_Applications`

[2] L. Liu, Z. Huang: A note on Mori-Tanaka's method, *Acta Mechanica Solida Sinica*, 27(3):234-244, 2014; DOI: `https://doi.org/10.1016/S0894-9166(14)60033-1`

[3] `https://omnexus.specialchem.com/selection-guide/polybutylene-terephthalate-pbt-plastic`; accessed 26 April 2019.

[4] `https://www.campusplastics.com/campus/en/datasheet/Pocan+B1305+000000/LANXESS/99/a5c1c937/SI?pos=0`; accessed 7 June 2019.

[5] `https://www.campusplastics.com/campus/en/datasheet/Pocan+B3225+000000/LANXESS/99/9d2ca065/SI?pos=273`; accessed 7 June 2019.

[6] `https://www.azom.com/properties.aspx?ArticleID=1998`; accessed 7 June 2019.

[7] R. Kleijnen *et al.*: Insights into the development of a short-fiber reinforced polypropylene for laser sintering, *AIP Conference Proceedings*, 1914(1):190002, 2017; DOI: `https://doi.org/10.1063/1.5016791`

[8] `https://www.azom.com/properties.aspx?ArticleID=764`; accessed 7 June 2019.

[9] `https://www.campusplastics.com/campus/en/datasheet/Pocan+B3235+000000/LANXESS/99/b121d29a/SI?pos=277`; accessed 7 June 2019.

[10] C.P. Okeke *et al.*: Hyperelastic polymer material models for robust fatigue performance of automotive LED lamps, *Procedia Structural Integrity*, 5:600-607, 2017; DOI: `https://doi.org/10.1016/j.prostr.2017.07.022`

[11] K. Wang *et al.*: Microstructures and fracture behavior of glass-fiber reinforced PBT/PC/E-GMA elastomer blends-1:microstructures, *Composites Science and Technology*, 61(11):1529-1538, 2001; DOI: `https://doi.org/10.1016/S0266-3538(01)00055-0`

[12] E.J. Barbero: Finite Element Analysis of Composite Materials Using Abaqus^{TM}, CRC Press, Taylor & Francis Group, Boca Raton, 2013, pp. 17-24, 35-89, 215-247.

[13] P. Kelly: Solid Mechanics Part I - An Introduction to Solid Mechanics, Auckland: The University of Auckland, 2013, pp. 156-166.
Available online at:
`http://homepages.engineering.auckland.ac.nz/~pkel015/SolidMechanicsBooks/Part_I/index.html`; accessed 3 May 2019.

[14] M. Trapp, A. Öchsner: Computational Plasticity for Finite Elements, A Fortran-Based Introduction, Springer International Publishing, Switzerland, 2018; DOI: `https://doi.org/10.1007/978-3-319-77206-6`

[15] K. Chung, M.G. Lee: Basics of Continuum Plasticity, Springer Nature Singapore, Singapore, 2018, pp. 199-211; DOI: `https://doi.org/10.1007/978-981-10-8306-8`

[16] `https://en.wikipedia.org/wiki/Von_Mises_yield_criterion`; accessed 30 October 2019.

[17] Digimat 5.1.1 documentation, e-Xstream Engineering, 2014, pp. 149-181.

[18] D. Broek: The Practical Use of Fracture Mechanics, Kluwer Academic Publishers, Dordrecht, 1989, pp. 102-106.

[19] Abaqus 6.14 documentation collection, Dassault Systèmes, 2014.

[20] B. Mortazavi *et al.*: Modeling of two-phase random composite materials by finite element, Mori-Tanaka and strong contrast methods, *Composites Part B: Engineering*, 45(1):1117-1125, 2013; DOI: `https://doi.org/10.1016/j.compositesb.2012.05.015`

[21] O. Pierard *et at.*: Micromechanics of elasto-plastic materials reinforced with ellipsoidal inclusions, *International Journal of Solids and Structures*, 44(21):6945-6962, 2007; DOI: `https://doi.org/10.1016/j.ijsolstr.2007.03.019`

[22] L. Brassart, I. Doghri, and L. Delannay: Homogenization of elasto-plastic composites coupled with a nonlinear finite element analysis of the equivalent inclusion problem, *International Journal of Solids and Structures*, 47(5):716-729, 2010, DOI: `https://doi.org/10.1016/j.ijsolstr.2009.11.013`

[23] J.D. Eshelby: The determination of the elastic field of an ellipsoidal inclusion, and related problems, *Proceedings of the Royal Society of London*, 241(1226):376-396, 1957; DOI: `https://doi.org/10.1098/rspa.1957.0133`

[24] I. Doghri, L. Tinel: Micromechanics of inelastic composites with misaligned inclusions: Numerical treatment of orientation, *Computer Methods in Applied Mechanics and Engineering*, 195:1387-1406, 2006; DOI: `https://doi.org/10.1016/j.cma.2005.05.041`

[25] I. Doghri, L. Tinel: Micromechanical modeling and computation of elasto-plastic materials reinforced with distributed-orientation fibers, *International Journal of Plasticity*, 21(10):1919-1949, 2005; DOI: `https://doi.org/10.1016/j.ijplas.2004.09.003`

[26] D. Gross, T. Seelig: Fracture Mechanics, With an Introduction to Micromechanics, Springer International Publishing, Switzerland, 2018, pp. 243-313; DOI: `https://doi.org/10.1007/978-3-319-71090-7`

[27] I. Doghri, C. Friebel: Effective elasto-plastic properties of inclusion-reinforced composites. Study of shape, orientation and cyclic response, *Mechanics of Materials*, 37(1):45-68, 2005, DOI: `https://doi.org/10.1016/j.mechmat.2003.12.007`

[28] B. Klusemann, H.J. Böhm, and B. Svendsen: Homogenization methods for multi-phase elastic composites with non-elliptical reinforcements: Comparisons and benchmarks, *European Journal of Mechanics-A/Solids*, 34(0):21-37, 2012, DOI: `https://doi.org/10.1016/j.euromechsol.2011.12.002`

[29] I.Doghri, A. Quaar: Homogenization of two-phase elasto-plastic composite materials and structures: Study of tangent operators, cyclic plasticity and numerical algorithms, *International Journal of Solids and Structures* , 40(7):1681-1712, 2003, DOI: `https://doi.org/10.1016/S0020-7683(03)00013-1`

[30] T. Mori, K. Tanaka: Average stress in matrix and average elastic energy of materials with misfitting inclusions, *Acta Metallurgica*, 21(5):571-574, 1973; DOI: `https://doi.org/10.1016/0001-6160(73)90064-3`

[31] H. Tan *et at.*: The Mori-Tanaka method for composite materials with nonlinear interface debonding, *International Journal of Plasticity*, 21:1890-1918, 2005; DOI: `https://doi.org/10.1016/j.ijplas.2004.10.001`

[32] Y. Benveniste: A new approach to the application of Mori-Tanaka theory in composite materials, *Mechanics of Materials*, 6:147-157, 1989.;
Available online at:
`https://scholar.google.hr/scholar?hl=hr&as_sdt=0%2C5&q=A+new+approach+to+the+application+of+Mori-Tanaka+theory+in+composite+materials&btnG=`; accessed: 11 June 2019.

[33] S.V. Lomov *et al.*: Mori-Tanaka methods for micromechanics of random fibre composites, *International Conference on Composite Materials*, 2015.
Available online at:
`https://www.researchgate.net/publication/280626987_MORI-TANAKA_METHODS_FOR_MICROMECHANICS_OF_RANDOM_FIBRE_COMPOSITES`

[34] P. Sadowski *et al.*: Consistent treatment and automation of the incremental Mori–Tanaka scheme for elasto-plastic composites, *Computational Mechanics*, 60(3):493-511, 2017; DOI: `https://doi.org/10.1007/s00466-017-1418-z`

[35] L. Cheng *et al.*: A stress-based variational model for ductile porous materials, *International Journal of Plasticity*, 55:133-151, 2014; DOI: `https://doi.org/10.1016/j.ijplas.2013.10.003`

[36] M.I. El Ghezal *et al.*: Static limit analysis and strength of porous solids with hill orthotropic matrix, *International Journal of Solids and Structures*, 109:63-71, 2017; DOI: `https://doi.org/10.1016/j.ijsolstr.2017.01.007`

[37] M.I. El Ghezal, I. Doghri: Porous plasticity: predictive second moment homogenization models coupled with Gurson's single cavity stress-strain solution, *International Journal of Plasticity*, 108:201-221, 2018; DOI: `https://doi.org/10.13140/RG.2.2.25460.65927`

[38] T.I. Zohdi: A Finite Element Primer for Beginners: The Basics, Springer International Publishing, Switzerland, 2018; DOI: `https://doi.org/10.1007/978-3-319-70428-9`

[39] O. Vestrum *et al.*: Finite element modeling of porous polymer pipeline coating using X-ray micro computed tomography, *Composites Part B: Engineering*, 172:406-415, 2019; DOI: `https://doi.org/10.1016/j.compositesb.2019.04.028`

Appendix A

A.1: Linear regression-isotropic hardening parameters

linear_regression.py

```
import numpy as np
from scipy import optimize


def power_law(e_tot, G_tot):
    '''
    Determines the coefficients k and m of the power law
    equation Rp(p) = k*p**m.
    e_tot: array, total strain values in the plastic regime,
           1st element is the yield strain value
    G_tot: array, stress values in the plastic regime,
           1st element is the yield stress value
    '''
    Gy = G_tot[0]
    e_el = e_tot[0]

    p = (e_tot - e_el) / 100
    # if the strain values are decimal already,
    # remove the division by 100
    p = np.delete(p, 0)
    # removes the 1st element which is zero;
    # eliminates a runtime error,
    # doesn't change the obtained parameters

    Rp = G_tot - Gy
    Rp = np.delete(Rp, 0)

    popt, pcov = optimize.curve_fit(
        lambda t, k0, m0: k0 * t ** m0, p, Rp, p0=(5, 0.1))
        # p0 - initial guess
    k, m = popt[0], popt[-1]
    print('k = ', round(k, 3), '\nm = ', round(m, 6))


```

```
if __name__ == '__main__':

    e_tot = np.array([2.0582, 2.1971, 2.3625, 2.5798, 2.8773,
                      3.2531, 3.6592, 4.0667, 4.4738, 4.8807,
                      5.2877, 5.6948, 6.1019, 6.5093, 6.9169,
                      7.3246, 7.7325, 8.1404, 8.5484, 8.9566,
                      9.3647, 9.773, 10.1813])
                      # strains are in percent

    G_tot = np.array([49.459, 51.5, 53.574, 55.726, 57.751,
                      59.12, 59.608, 59.639, 59.7, 59.858,
                      60.073, 60.309, 60.526, 60.695, 60.817,
                      60.904, 60.966, 61.014, 61.057, 61.098,
                      61.136, 61.174, 61.21])

    power_law(e_tot, G_tot)
```

A.2: Coupled Digimat-Abaqus analysis

An example of an input file for a coupled Digimat-Abaqus analysis is shown. For simplicity, only the general layout is shown, with the actual model definitions omitted. The model is defined in Abaqus and an input file is generated. Then, only the material is called from files generated in Digimat CAE. Parts which have to be added to the input file have been marked in color. The material name in section and material definition has to be the same as in the generated Digimat files. For the analysis to complete successfully, the files containing information about the material have to be in the same working directory as the input file when the job is executed. The **Depvar* keyword is used to define the number of internal state variables for a user-defined material. Then the internal state variables are defined. In this input file example, a reduced number of internal state variables is defined. For all the available state variables in Digimat, refer to [17]. Finally, the output of the defined state variables is requested through the **Element output* command. The *EVOL* parameter makes it possible to obtain volume average values.

tension_specimen.inp

```
** Tension-Specimen
*Heading
*Preprint, echo=NO, model=NO, history=NO, contact=NO
**
** PARTS
**
*Part, name=Tension_Specimen
*Node
**
** Nodes
**
*Element, type=C3D20R
**
** Elements
**
*Node
   1549,           0.,          75.,
*Elset, elset=Set-2, generate
   1,  190,    1
** Section: Section-1
*Solid Section, elset=Set-2, material=PBT08Pores
,
*End Part
**
** ASSEMBLY
**
*Assembly, name=Assembly
**
*Instance, name=Tension_Specimen-1, part=Tension_Specimen
*End Instance
*End Assembly
**
** MATERIALS
**
*Material, name=PBT08Pores
*User Material, Type = mechanical, constants = 1
0.,
```

```
*Depvar
12
1,"001_E11_macro","Average macro 11-strain"
2,"002_E22_macro","Average macro 22-strain"
3,"003_E33_macro","Average macro 33-strain"
4,"004_2*E12_macro","2 * Average macro 12-strain"
5,"005_2*E23_macro","2 * Average macro 23-strain"
6,"006_2*E13_macro","2 * Average macro 13-strain"
7,"007_S11_macro","Average macro 11-Cauchy stress"
8,"008_S22_macro","Average macro 22-Cauchy stress"
9,"009_S33_macro","Average macro 33-Cauchy stress"
10,"010_S12_macro","Average macro 12-Cauchy stress"
11,"011_S23_macro","Average macro 23-Cauchy stress"
12,"012_S13_macro","Average macro 13-Cauchy stress"
**
** BOUNDARY CONDITIONS
**
**
** OUTPUT REQUESTS
**
*Restart, write, frequency=0
**
** FIELD OUTPUT: F-Output-1
**
*Output, field, variable=PRESELECT
*Element output
SDV, EVOL
**
** HISTORY OUTPUT: H-Output-1
**
*Output, history, variable=PRESELECT
*End Step
```